ZAMM · Z. Angew. Math. Mech. **97**, No. 11, 1358–1380 (2017) / **DOI** 10.1002/zamm.201600010

A comparison of explicit and semi-implicit finite volume schemes for viscous compressible flows in elastic pipes in fast transient regime

Matteo Ioriatti[1],*, **Michael Dumbser**[1],**, **and Uwe Iben**[2],***

[1] University of Trento, Via Mesiano 77, 38123 Trento, Italy
[2] Robert Bosch GmbH, Postfach 10 60 50, D-70049 Stuttgart, Germany

Received 22 January 2016, revised 5 November 2016, accepted 23 May 2017
Published online 13 June 2017

Key words Finite volume schemes, explicit path conservative schemes, semi-implicit staggered schemes, viscous compressible laminar flow in elastic tubes, unsteady friction models, highly oscillatory flow, water hammer.

This paper compares the accuracy and computational efficiency of fully explicit and semi-implicit 1D and 2D finite volume schemes for the simulation of highly unsteady viscous compressible flows in laminar regime in axially symmetric compliant tubes. There are essentially two main classes of mathematical models that can be used to predict the pressure and velocity distribution along the tube: one class is based on the full compressible Navier-Stokes equations in an axially symmetric geometry, leading to a two-dimensional governing PDE system with moving boundaries, and the other class uses a simpler, cross-sectionally averaged version of the Navier-Stokes equations, which leads to a non-conservative PDE system in only one space dimension along the axial direction of the tube. Within the first class of models, the influence of the wall friction on the flow field is directly obtained from first principles, without any further modelling assumptions and is thus valid even for highly unsteady flows. In the second case, only averaged flow quantities are available, and it is well known from previous studies published in the literature that the correct representation of the wall friction needs to be *frequency dependent*, since the use of a simple steady friction model, like the classical Darcy-Weisbach law, is not sufficient to reproduce the wall friction effects in highly transient flows. For the cross-sectionally averaged Navier-Stokes equations, there are again two main classes of frequency-dependent wall friction models: convolution integral (CI) models and instantaneous acceleration (IA) models.

In this paper we provide a very thorough and critical comparison of all the above-mentioned methods for the simulation of highly oscillatory flows in rigid and compliant tubes concerning accuracy and computational efficiency. From our numerical results we can conclude that the convolution integral models are significantly superior to instantaneous acceleration models concerning accuracy. Furthermore, the CI models require only a slight computational overhead if they are properly implemented by solving a set of additional ODEs for appropriate auxiliary variables, instead of directly computing the convolution integrals. We also find that semi-implicit finite volume methods are clearly superior to conventional explicit finite volume schemes concerning computational efficiency, however, providing the same level of accuracy.

1 Introduction

Unsteady pressurized viscous flows in systems of rigid and compliant ducts with circular cross section have a very wide range of practical applications and are therefore of great interest for theoretical and computational fluid dynamics. Some important examples are: blood flow in systems of arteries and veins of the human cardiovascular system, flow in aqueducts of complex urban water supply networks, pressurized pipe flow in hydroelectric power plants, flow in oil and gas pipelines and industrial flows in devices such as pumps, fuel injectors and breaking system. All these phenomena can be in principle described by the fully three-dimensional compressible or incompressible Navier-Stokes equations, both of which are coupled nonlinear systems of partial differential equations (PDE). However, these PDE systems admit analytic solutions only in very simple cases and for very special initial and boundary conditions. Consequently, a computational approach is necessary to reproduce realistic situations and very often simplified 2D and 1D models are adopted in order to increase the efficiency of the numerical simulations.

In this paper, we compare different mathematical models and different numerical methods with each other, in order to cover a very wide range of existing computational methods for compressible pipe flow. In this paper, we restrict ourselves to *laminar flows* that occur very often both in hemodynamics and in industrial engineering at small radial scales. First, an

* Corresponding author: E-mail: matteo.ioriatti@unitn.it, Phone: +39 0461 28 26 89
** e-mail: michael.dumbser@unitn.it
*** e-mail: uwe.iben@de.bosch.com

explicit finite volume method is considered for the solution of a 1D cross-sectionally averaged model of viscous compressible flows in compliant pipes. The governing PDE system is hyperbolic, but it also contains important non-conservative terms and friction source terms. Such hyperbolic PDE with non-conservative products are conveniently discretized at the aid of so-called *path-conservative* finite volume schemes, which have been originally introduced by Castro and Parés and their co-workers for shallow water-type equations, see e.g.[5, 7, 27]. The path-conservative framework naturally leads to so-called *well-balanced schemes*, which preserve some special steady state solutions at rest exactly. This property is very important also in the case of flow in pipes with varying cross section. The Riemann problem for averaged 1D models has been discussed in great detail in [19,29]. In our particular case, the numerical solution of the governing PDE system is found at the aid of two approximate Riemann solvers that have been very recently extended to the path-conservative framework, namely the Osher-Solomon Riemann solver and the HLLEM Riemann solver, see [13, 16, 22]. A new interesting variant of Osher-type Riemann solvers that does not need the full eigenstructure of the PDE system but which relies on a polynomial viscosity matrix (PVM) has been very recently forwarded in [6].

Afterwards, a second class of numerical schemes is considered for the solution of the cross-sectionally averaged 1D model, namely a *semi-implicit* finite volume method on *staggered grids* that was originally developed for the simulation of incompressible flows in systems of compliant arteries in [32] and which has been recently extended also to the compressible case in [14]. In this paper, also the strategy for properly including the friction source term into the scheme is explained. Finally, we also briefly recall the semi-implicit 2D model presented in [14], which is directly based on first principles and which will therefore be used as a reference, in order to analyze the accuracy and the efficiency of the methods used to solve the simplified cross-sectionally averaged 1D model.

In this paper, great attention is dedicated to the influence of the wall friction. While for the 2D model the radial velocity profile is available and therefore the viscous term can be discretized directly without any simplifications, for cross-sectionally averaged 1D models it is necessary to introduce a closure relation in order to take into account the friction effects. Moreover, for phenomena characterized by rapid transients, one must also take into account the unsteady component of the wall shear stress, which is given by the solution of the convolution integral of Zielke [41]. The direct calculation of this contribution is in general very expensive from the computational point of view. In this work we first recall existing alternative strategies and then we also propose a new and very efficient approximation of the convolution integral by solving additional ordinary differential equations (ODEs) for appropriate auxiliary variables.

This paper is structured as follows: in Sect. 2 the main mathematical and numerical aspects of the considered methods are recalled and the new approximation of the unsteady friction model is exposed. In Sect. 3 the numerical methods are applied to different test cases. Their outputs are compared against several analytic solutions and against experimental data. Finally, the computational efficiency of all numerical schemes is analyzed and compared. The paper closes with some concluding remarks in Sect. 4.

2 Mathematical models and numerical methods for pipe flow

2.1 Explicit path-conservative finite volume schemes for non-conservative hyperbolic systems

After having taken a cross-sectional average of the 3D compressible Navier-Stokes equations in an axially symmetric duct, the flow of a viscous and compressible fluid in a flexible duct can be modeled by a simplified system of 1D partial differential equations (PDE) which is composed by the continuity and by the momentum equation. It is written as follows:

$$\begin{aligned} &\frac{\partial}{\partial t}(\rho A) + \frac{\partial}{\partial x}(\rho A U) = 0, \\ &\frac{\partial}{\partial t}(\rho A U) + \frac{\partial}{\partial x}(\rho A U^2 + A p) = p\frac{\partial A}{\partial x} - 2\pi R \tau_w, \end{aligned} \tag{1}$$

where $t \in \mathbb{R}_0^+$ is the time, x is the longitudinal coordinate which belongs to the 1D domain $\Omega = [x_L, x_R] \subset \mathbb{R}$, ρ is the density, A is the cross sectional area of the tube, U is the mean velocity in the x direction, p is the mean pressure and τ_w is the wall shear stress. This system is composed by two equations but it has five unknowns. Consequently three closure relations need to be introduced. The first one relates the pressure with density; here, we use a simple equation of state that is valid for a barotropic fluid:

$$p = p(\rho) = p_0 + c_0^2 (\rho - \rho_0), \tag{2}$$

where ρ_0, p_0, and c_0 are the reference density, pressure, and speed of sound of the fluid, respectively. The second closure relation connects the cross sectional area of the pipe with the pressure. Here we use a simple elastic model which is given by Hooke's law applied to a cross sectional area of a pipe [18, 23]:

$$A = \pi R^2, \quad R = R_0\sqrt{1 + \frac{2Wp}{E_\infty}}. \tag{3}$$

In Eq. (3), R_0 is the equilibrium radius, E_∞ is the Young's modulus of the material and W is a geometric parameter which contains the dependence on the wall thickness h_w and the Poisson ratio ν_w of the tube, see [18, 23]:

$$W = 2\frac{\left(\frac{h_w}{R_0}\right)^2(1+\nu_w) - (1-2\nu_w)}{\left(\frac{h_w}{R_0}\right)^{2-1}}. \tag{4}$$

In this paper the material parameters h_w and ν_w are assumed to be constant. Note that when E_∞ tends to infinity the tubes become stiff and, consequently, the wall strain is very small. The last closure regards the evaluation of τ_w. In experiments characterized by fast transient flow the classical Darcy-Weisbach formula, valid for the stationary regime, for the computation of the tangential stress has to be supplemented by an additional term which contains the unsteady friction component. Under the assumption of laminar flow the total wall shear stress is computed as $\tau_w = \tau_s + \tau_u$. Here, τ_s is the quasi-steady friction term expressed as $\tau_s = \rho\lambda|U|U/8$, with $\lambda = 64/\mathrm{Re}$ being the usual Darcy-Weisbach friction factor for laminar flows given in terms of the Reynolds number Re and τ_u is the unsteady wall shear stress. Its evaluation is discussed in detail in Sect. 2.3. Note that when $\partial A/\partial x = 0$ and $\tau_w = 0$ in (1), one obtains the well known 1D compressible Euler equations for barotropic fluids.

Introducing the vector of the conserved variables defined as $\mathbf{Q} = (\rho A, \rho AU)^T$, system (1) can be written as follows:

$$\frac{\partial \mathbf{Q}}{\partial t} + \mathbf{J}(\mathbf{Q})\frac{\partial \mathbf{Q}}{\partial x} + \mathbf{B}(\mathbf{Q})\frac{\partial \mathbf{Q}}{\partial x} = \mathbf{S}(\mathbf{Q}), \tag{5}$$

where $\mathbf{J}(\mathbf{Q}) = \partial\mathbf{f}(\mathbf{Q})/\partial\mathbf{Q}$ is the Jacobian matrix of the flux vector $\mathbf{f} = (\rho AU, \rho AU^2 + Ap)^T = (Q_2, Q_2^2/Q_1 + Ap)^T$. $\mathbf{B}(\mathbf{Q})\partial\mathbf{Q}/\partial x$ represents the non-conservative term and the only non-zero element of the matrix $\mathbf{B}$ is B_{21} which is equal to $B_{21} = p/(\frac{A}{c_0^2\partial A/\partial p} + \rho)$; $\mathbf{S}(\mathbf{Q})$ is the source term and the non-zero term is given by the total wall shear stress that has to be properly written in conserved variables. It is possible to introduce the matrix $\mathbf{A}(\mathbf{Q}) = \mathbf{J}(\mathbf{Q}) + \mathbf{B}(\mathbf{Q})$ and rewrite the system (5) as a quasi-linear system of PDEs as follows

$$\frac{\partial \mathbf{Q}}{\partial t} + \mathbf{A}(\mathbf{Q})\frac{\partial \mathbf{Q}}{\partial x} = \mathbf{S}(\mathbf{Q}). \tag{6}$$

The diagonal matrix of eigenvalues $\mathbf{\Lambda} = \mathrm{diag}(\lambda_1, \lambda_2)$ and the matrix of right eigenvectors $\mathbf{R}$ of the matrix $\mathbf{A}$ read

$$\mathbf{\Lambda} = \begin{bmatrix} U - c' & 0 \\ 0 & U + c' \end{bmatrix} \quad \mathbf{R} = \begin{bmatrix} 1 & 1 \\ U - c' & U + c' \end{bmatrix} \quad \text{with} \quad c' = \frac{c_0}{\sqrt{1 + \frac{\rho c_0^2}{A}\frac{\partial A}{\partial p}}}, \tag{7}$$

where the parameter c' is the speed of sound modified by the effect of the wall elasticity and the derivative $\partial A/\partial p$ can be directly derived from Eq. (3). Furthermore, it is important to remind that in the flux calculation the pressure has to be found from the known conservative quantities by solving the nonlinear scalar equation $g(p) = Q_1 - \rho(p)A(p) = 0$. In order to do this one can either use a Newton method or the more robust bisection method.

A grid composed by N_x equally spaced intervals $T_i = [x_{i-\frac{1}{2}}, x_{i+\frac{1}{2}}]$ is introduced; the length of each element T_i is equal to $\Delta x = x_{i+\frac{1}{2}} - x_{i-\frac{1}{2}} = (x_L - x_R)/N_x$. The finite volume update based on a second order space-time TVD reconstruction for a non-conservative system of hyperbolic equations reads (see [13])

$$\mathbf{Q}_i^{n+1} = \mathbf{Q}_i^n - \frac{\Delta t}{\Delta x}\left(\mathbf{D}^-_{i+\frac{1}{2}} + \mathbf{D}^+_{i-\frac{1}{2}}\right) - \frac{\Delta t}{\Delta x}\left(\mathbf{f}^-_{i+\frac{1}{2}} - \mathbf{f}^+_{i-\frac{1}{2}}\right) - \frac{\Delta t}{\Delta x}\mathbf{B}(\mathbf{Q}_i^{n+\frac{1}{2}})\Delta\mathbf{Q}_i^n + \Delta t\mathbf{S}(\mathbf{Q}_i^{n+\frac{1}{2}}), \tag{8}$$

where the $\mathbf{D}^\pm_{i+\frac{1}{2}}$ are the so-called fluctuations and $\mathbf{f}^\pm_{i+\frac{1}{2}} = \mathbf{f}(\mathbf{Q}^{n+\frac{1}{2},\pm}_{i+\frac{1}{2}})$ are the boundary extrapolated fluxes from within the element. The $\Delta\mathbf{Q}_i^n$ are the slopes computed from the cell averages at time t^n by using the standard MINMOD slope limiter (applied componentwise) [33]

$$\Delta\mathbf{Q}_i^n = \mathrm{minmod}(\mathbf{Q}_{i+1}^n - \mathbf{Q}_i^n, \mathbf{Q}_i^n - \mathbf{Q}_{i-1}^n). \tag{9}$$

Once that reconstructed values $\mathbf{Q}_{i\pm\frac{1}{2}}^{n,\mp} = \mathbf{Q}_i^n \pm \Delta\mathbf{Q}_i^n$ at the time t^n are known, the quantities at the boundary and at the half time $t^{n+\frac{1}{2}} = t^n + \frac{1}{2}\Delta t^n$ are given by the following time evolution:

$$\partial_t \mathbf{Q}_i^n = -\frac{\left(\mathbf{f}\left(\mathbf{Q}_{i+\frac{1}{2}}^{n,-}\right) - \mathbf{f}(\mathbf{Q}_{i-\frac{1}{2}}^{n,+})\right)}{\Delta x} - \mathbf{B}(\mathbf{Q}_i^n)\frac{\Delta\mathbf{Q}_i^n}{\Delta x} + \mathbf{S}\left(\mathbf{Q}_i^n\right), \quad \mathbf{Q}_{i\pm\frac{1}{2}}^{n+\frac{1}{2},\mp} = \mathbf{Q}_i^n \pm \frac{1}{2}\Delta\mathbf{Q}_i^n + \frac{\Delta t}{2}\partial_t\mathbf{Q}_i^n. \tag{10}$$

We furthermore have used the abbreviation $\mathbf{Q}_i^{n+\frac{1}{2}} = \mathbf{Q}_i^n + \frac{1}{2}\Delta t\,\partial_t\mathbf{Q}_i^n$. Then, the fluctuations $\mathbf{D}_{i+\frac{1}{2}}^{\pm}$ can be computed by using either the Osher Riemann solver [25,26] or the HLL Riemann solver, both extended to non-conservative systems of hyperbolic equations using the path-conservative framework of Castro and Parés [5,27]:

$$\mathbf{D}_{i+\frac{1}{2}}^{\pm} = \mathbf{D}_{\mathbf{OSHER}}^{\pm}\left(\mathbf{Q}_{i+\frac{1}{2}}^{n+\frac{1}{2},-}, \mathbf{Q}_{i+\frac{1}{2}}^{n+\frac{1}{2},+}\right) \quad \text{or} \quad \mathbf{D}_{i+\frac{1}{2}}^{\pm} = \mathbf{D}_{\mathbf{HLL}}^{\pm}\left(\mathbf{Q}_{i+\frac{1}{2}}^{n+\frac{1}{2},-}, \mathbf{Q}_{i+\frac{1}{2}}^{n+\frac{1}{2},+}\right). \tag{11}$$

We recall that for the path-conservative Osher scheme [16] the jump terms for two general states $\mathbf{Q_L}$ and $\mathbf{Q_R}$ read

$$\mathbf{D}_{\mathbf{OSHER}}^{\pm}(\mathbf{Q_L}, \mathbf{Q_R}) = \frac{1}{2}\left(\int_0^1 \mathbf{A}(\boldsymbol{\psi}(s))ds \pm \int_0^1 |\mathbf{A}(\boldsymbol{\psi}(s))|ds\right)(\mathbf{Q_R} - \mathbf{Q_L}), \tag{12}$$

when using the simple segment path $\boldsymbol{\psi}(\mathbf{Q_L}, \mathbf{Q_R}, s) = \mathbf{Q_L} + s(\mathbf{Q_R} - \mathbf{Q_L})$. However, the path integral appearing in the expression above can become quite cumbersome to evaluate for general PDE systems. With an abuse of notation, throughout the rest of the paper we therefore define $\mathbf{D}_{\mathbf{OSHER}}^{\pm}(\mathbf{Q_L}, \mathbf{Q_R})$ to be the *approximation* of (12) via *numerical quadrature*, i.e. as

$$\mathbf{D}_{\mathbf{OSHER}}^{\pm}(\mathbf{Q_L}, \mathbf{Q_R}) = \frac{1}{2}\sum_j^G w_j\left(\mathbf{A}(\boldsymbol{\psi}(s_j)) \pm \left|\mathbf{A}(\boldsymbol{\psi}(s_j))\right|\right)(\mathbf{Q_R} - \mathbf{Q_L}), \tag{13}$$

where the path integral has been approximated using a Gauss-Legendre integration rule with nodes s_j and weights w_j on the unit interval $[0, 1]$. For systems composed of only two PDEs, as the one considered in (1), the HLLEM Riemann solver proposed in [13] reduces to the HLL method, for which the jumps term (fluctuations) are given by the expressions

$$\begin{aligned}
\mathbf{D}_{\mathbf{HLL}}^{-}(\mathbf{Q_L}, \mathbf{Q_R}) &= -\frac{s_L}{s_R - s_L}\left[\mathbf{f}_R - \mathbf{f}_L + \mathbf{D}_*\right] + \frac{s_L s_R}{s_R - s_L}(\mathbf{Q_R} - \mathbf{Q_L}),\\
\mathbf{D}_{\mathbf{HLL}}^{+}(\mathbf{Q_L}, \mathbf{Q_R}) &= +\frac{s_R}{s_R - s_L}\left[\mathbf{f}_R - \mathbf{f}_L + \mathbf{D}_*\right] - \frac{s_L s_R}{s_R - s_L}(\mathbf{Q_R} - \mathbf{Q_L}),
\end{aligned} \tag{14}$$

with the abbreviation $\mathbf{D}_* = \tilde{\mathbf{B}}(\mathbf{Q_L}, \mathbf{Q}_*)(\mathbf{Q}_* - \mathbf{Q}_L) + \tilde{\mathbf{B}}(\mathbf{Q}_*, \mathbf{Q_R})(\mathbf{Q}_R - \mathbf{Q}_*)$ and where $\mathbf{Q}_*$ is the intermediate HLL state computed as

$$\mathbf{Q}_* = \frac{1}{s_R - s_L}\left[(\mathbf{Q_R}s_R - \mathbf{Q_L}s_L) - (\mathbf{f}_R - \mathbf{f}_L) - \tilde{\mathbf{B}}(\mathbf{Q_L}, \mathbf{Q_R})(\mathbf{Q}_R - \mathbf{Q}_L)\right], \tag{15}$$

and for $\tilde{\mathbf{B}}(\mathbf{Q_a}, \mathbf{Q_b})$ we have

$$\tilde{\mathbf{B}}(\mathbf{Q_a}, \mathbf{Q_b}) = \int_0^1 \mathbf{B}(\boldsymbol{\psi}(\mathbf{Q_a}, \mathbf{Q_b}, s))ds = \sum_j^G w_j \mathbf{B}(\boldsymbol{\psi}(s_j))(\mathbf{Q_a} - \mathbf{Q_b}). \tag{16}$$

The wave speeds are estimated according to [13] as follows,

$$s_L = \min(0, \boldsymbol{\Lambda}(\mathbf{Q_L}), \boldsymbol{\Lambda}(\tilde{\mathbf{Q}})) \quad s_R = \max(0, \boldsymbol{\Lambda}(\mathbf{Q_R}), \boldsymbol{\Lambda}(\tilde{\mathbf{Q}})) \quad \text{with } \tilde{\mathbf{Q}} = \frac{1}{2}(\mathbf{Q_R} + \mathbf{Q_R}), \tag{17}$$

with $\min(0, \boldsymbol{\Lambda}, \tilde{\boldsymbol{\Lambda}}) = \min(0, \lambda_1, \lambda_2, \tilde{\lambda}_1, \tilde{\lambda}_2)$ and $\max(0, \boldsymbol{\Lambda}, \tilde{\boldsymbol{\Lambda}}) = \max(0, \lambda_1, \lambda_2, \tilde{\lambda}_1, \tilde{\lambda}_2)$. As already mentioned above, in Eq. (13) and Eq. (16), s_j and w_j are the points and weights of an appropriate Gauss-Legendre quadrature formula. In this paper $G = 3$ and consequently $s = (\frac{1}{2} - \frac{\sqrt{15}}{10}, \frac{1}{2}, \frac{1}{2} + \frac{\sqrt{15}}{10})$ and $w = (\frac{5}{18}, \frac{8}{18}, \frac{5}{18})$. For all the details see [16]. The scheme obeys the stability condition $\Delta t = \mathrm{CFL}\frac{\Delta x}{\max|\boldsymbol{\Lambda}(\mathbf{Q_i^n})|}$ with $\mathrm{CFL} \leq 1$ and it is second order of accuracy both in space and in time. This stability condition is based on the speed of sound of the flow, but for incompressible flows, the ratio of flow speed and sound speed (the Mach number) tends to infinity. This means that in the incompressible limit explicit time stepping schemes become increasingly inefficient and a different strategy, such as the semi-implicit approach explained in [12,14], has to be introduced in order to perform faster simulations.

Furthermore, as shown in [13,22], the path-conservative HLLEM scheme and the path-conservative Osher Riemann solver are well balanced for certain classes of non-conservative PDE systems. In particular, these schemes exactly preserve steady state solutions with zero velocity and constant pressure in ducts with variable reference cross section ($A_0 = \pi R_0^2$)

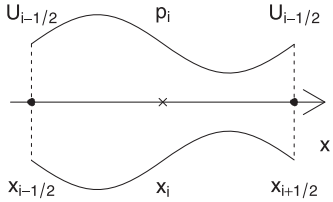

Fig. 1 Grid for the semi-implicit 1D scheme: according to the staggered approach, the pressure is defined in the cell barycenter while the velocity is defined in the cell edges.

in longitudinal direction. However, in this paper for the sake of simplicity we only consider the case $R_0 = \text{const}$, since the main focus of this paper is on the detailed study of the influence of the wall friction in highly transient flows.

2.2 Semi-implicit finite volume schemes

In order to increase the computational efficiency of the simulation, especially for low Mach number flows, an alternative semi-implicit discretization can be used in order to approximate the PDE system (1). Here it is rewritten as follows for convenience:

$$\frac{\partial}{\partial t}(\rho A) + \frac{\partial}{\partial x}(\rho A U) = 0, \tag{18a}$$

$$\frac{\partial}{\partial t}(\rho A U) + \frac{\partial}{\partial x}(\rho A U^2) = -A\frac{\partial p}{\partial x} - 2\pi R\tau_s - 2\pi R\tau_u. \tag{18b}$$

First, a *staggered grid* is introduced in order to define the one-dimensional domain. Hence, the pipe of length L is divided into N_x intervals of constant length $\Delta x = L/N_x$. The pressure is located at the cell centers x_i, while the velocities and the mass fluxes are defined at the interfaces $x_{i\pm\frac{1}{2}}$ of the control volumes (see Fig. 1). In addition, the θ-method is introduced for the time discretization, where θ is an implicitness parameter taken in the range $0.5 \le \theta \le 1$ for stability. Moreover when $\theta = 1$ the scheme is of first order of accuracy in time, while when $\theta = 0.5$ one has a Crank-Nicolson type scheme of second order. For example, the θ-method applied to the pressure $p_i^{n+\theta}$ gives $\theta p_i^{n+1} + (1-\theta)p_i^n$. The θ-method is widely used in the semi-implicit schemes (see [8, 12, 14, 17, 30, 32]) because is it quite a simple and cheap strategy to achieve second order of accuracy in time.

The semi-implicit discretization for the continuity equation yields [14]

$$M(p_i^{n+1}) = M\big(p_i^n\big) - \Delta t\left(Q_{i+\frac{1}{2}}^{n+\theta} - Q_{i-\frac{1}{2}}^{n+\theta}\right), \tag{19}$$

where $M(p_i) = \rho(p_i)A(p_i)\Delta x$ is the mass of fluid contained in the i-th cell and $Q_{i+\frac{1}{2}}^{n+1} = \rho_{i+\frac{1}{2}}^n A_{i+\frac{1}{2}}^n U_{i+\frac{1}{2}}^{n+1}$ is the mass flow rate with $\rho_{i+\frac{1}{2}}^n = \max[0, \frac{1}{2}\rho(p_i^n) + \frac{1}{2}\rho(p_{i+1}^n)]$ and $A_{i+\frac{1}{2}}^n = \max[0, \frac{1}{2}A(p_i^n) + \frac{1}{2}A(p_{i+1}^n)]$. At the same time, the discrete momentum equation reads

$$\frac{Q_{i+\frac{1}{2}}^{n+1} - FQ_{i+\frac{1}{2}}^n}{\Delta t} = -A_{i+\frac{1}{2}}^n\frac{\Delta t}{\Delta x}\big(p_{i+1}^{n+\theta} - p_i^{n+\theta}\big) - 2\pi R_{i+\frac{1}{2}}^n\rho_{i+\frac{1}{2}}^n\lambda_{i+\frac{1}{2}}^n\frac{U_{i+\frac{1}{2}}^n U_{i+\frac{1}{2}}^{n+1}}{8} - 2\pi R_{i+\frac{1}{2}}^n(\tau_u^n)_{i+\frac{1}{2}}, \tag{20}$$

where $FQ_{i+\frac{1}{2}}^n$ is an explicit and nonlinear operator for the convective terms. It can be computed in many ways and a simple choice can be a finite volume method based on the Rusanov flux, as done in [14]:

$$\begin{aligned} &FQ_{i+\frac{1}{2}}^n = Q_{i+\frac{1}{2}}^n - \frac{\Delta t}{\Delta x}\big(f_{i+1}^n - f_i^n\big), \quad \text{where} \\ &f_i = \frac{1}{2}\left(U_{i+\frac{1}{2}}^n Q_{i+\frac{1}{2}}^n + U_{i-\frac{1}{2}}^n Q_{i-\frac{1}{2}}^n\right) - \frac{1}{2}S_{\max}\left(Q_{i+\frac{1}{2}}^n - Q_{i-\frac{1}{2}}^n\right), \quad S_{\max} = 2\max\left(|U_{i-\frac{1}{2}}^n|, |U_{i+\frac{1}{2}}^n|\right). \end{aligned} \tag{21}$$

The evaluation of term τ_u^n is explained in Sect. 2.3. Eq. (20) can be rewritten as

$$Q_{i+\frac{1}{2}}^{n+1} = G_{i+\frac{1}{2}}^n - \theta A_{i+\frac{1}{2}}^n\frac{\Delta t}{\Delta x}\big(p_{i+1}^{n+1} - p_i^{n+1}\big) - \Delta t\gamma_{i+\frac{1}{2}}^n Q_{i+\frac{1}{2}}^{n+1}, \tag{22}$$

where the term $\gamma^n_{i+\frac{1}{2}} = \frac{2\pi R^n_{i+\frac{1}{2}} \lambda^n_{i+\frac{1}{2}} |U^n_{i+\frac{1}{2}}|}{8A^n_{i+\frac{1}{2}}} \geq 0$ takes into account the effects of quasi-steady friction using the Darcy-Weisbach law. Here $\lambda^n_{i+\frac{1}{2}} = 64/\mathrm{Re}$ denotes the (local) Darcy friction factor in terms of the Reynolds number of the flow. Moving $Q^{n+1}_{i+\frac{1}{2}}$ to the left hand side, the previous expression becomes

$$Q^{n+1}_{i+\frac{1}{2}} = \left(\frac{G}{1+\Delta t\gamma}\right)^n_{i+\frac{1}{2}} - \theta \frac{\Delta t}{\Delta x}\left(\frac{A}{1+\Delta t\gamma}\right)^n_{i+\frac{1}{2}} (p^{n+1}_{i+1} - p^{n+1}_i), \tag{23}$$

where the quantity $G^n_{i+\frac{1}{2}}$ includes the nonlinear convection and the known terms at time t^n:

$$G^n_{i+\frac{1}{2}} = F Q^n_{i+\frac{1}{2}} - (1-\theta) A^n_{i+\frac{1}{2}} \frac{\Delta t}{\Delta x}\left(p^n_{i+1} - p^n_i\right) - 2\pi R^n_{i+\frac{1}{2}} \left(\tau_u\right)^{n_{i+\frac{1}{2}}} \Delta t. \tag{24}$$

Substitution of Eq. (23) into Eq. (19) yields:

$$M\left(p^{n+1}_i\right) - \theta^2 \frac{\Delta t^2}{\Delta x}\left[\left(p^{n+1}_{i+1} - p^{n+1}_i\right)\left(\frac{A}{1+\Delta t\gamma}\right)^n_{i+\frac{1}{2}} - \left(p^{n+1}_i - p^{n+1}_{i-1}\right)\left(\frac{A}{1+\Delta t\gamma}\right)^n_{i-\frac{1}{2}}\right] = b^n_i, \tag{25}$$

which can be written more compactly using the following matrix vector notation

$$\mathbf{M}(\mathbf{p^{n+1}}) + \mathbf{T}\mathbf{p^{n+1}} = \mathbf{b}(\mathbf{p^n}), \tag{26}$$

where $\mathbf{M}$ is a vector function that contains the non-linearity, $\mathbf{T}$ is a symmetric three-diagonal matrix, $\mathbf{p^{n+1}}$ is the vector of the unknown pressures and $\mathbf{b^n}$ is the known right hand side term. System (26) is efficiently solved by using either the Newton algorithm of Brugnano and Casulli [1, 2], or the more general nested Newton algorithm of Casulli and Zanolli [9, 10, 14], if more complex equations of state are needed, see [12, 14]. When the pressure is known, the numerical mass flux can be easily computed by using Eq. (23) and, consequently, the new velocity is equal to $U^{n+1}_{i+\frac{1}{2}} = Q^{n+1}_{i+\frac{1}{2}}/(\rho^n_{i+\frac{1}{2}} A^n_{i+\frac{1}{2}})$. Moreover, the density and the cross sectional area at the new time are updated using the closures in Eq. (2) and in Eq. (3).

To improve the information that regards the radial velocity profile, one can use a semi-implicit scheme for a two-dimensional model such as the one suggested in [14]. This method is an extension to weakly compressible flows of the family of semi-implicit methods for blood flow presented in a series of recent papers [8, 17, 32]. Under the hypothesis of hydrostatic radial pressure equilibrium and when the longitudinal scale is much larger than the radial one, the motion of a compressible barotropic fluid in a circular elastic duct is described by the following system of equations, which is a simplification of the Navier-Stokes equation in cylindrical coordinates:

$$\begin{aligned} &\frac{\partial \rho r}{\partial t} + \frac{\partial}{\partial x}(\rho u r) + \frac{\partial}{\partial r}(\rho r w) = 0, \\ &\rho\left(\frac{\partial u}{\partial t} + u\frac{\partial u}{\partial x} + w\frac{\partial u}{\partial r}\right) = -\frac{\partial p}{\partial x} + \frac{\mu}{r}\frac{\partial}{\partial r}\left(r\frac{\partial u}{\partial r}\right), \end{aligned} \tag{27}$$

where r is the radial coordinate, μ is the dynamic viscosity, and u and w are the velocity components in x and r direction, respectively.

The kinematic boundary condition at the moving wall yields (see [8, 17, 32])

$$\frac{\partial R}{\partial t} + u\frac{\partial R}{\partial x} - w = 0 \quad \text{for} \quad r = R. \tag{28}$$

The first equation of system (27) is integrated over the cross section and using the kinematic boundary condition the following relation is obtained:

$$\frac{\partial \rho A}{\partial t} + 2\pi \frac{\partial}{\partial x}\int_0^R \rho u r \, dr = 0. \tag{29}$$

The quantities A and ρ can be computed by using the same closures introduced in the previous section. Similarly to the previous method, in axial direction there are N_x cells of length Δx and the pressure p_i is located at the center of these control volumes in the position x_i. The radial grid is composed of ring elements of size $\Delta r^n_{i+\frac{1}{2},k} = r^n_{i+\frac{1}{2},k+\frac{1}{2}} - r^n_{i+\frac{1}{2},k-\frac{1}{2}}$ with $k = 1, 2, \ldots, K^n_{i+\frac{1}{2}}$ where $K^n_{i+\frac{1}{2}}$ is the number of active rings at the cell interface $x_{i+\frac{1}{2}}$. $K^n_{i+\frac{1}{2}}$ is bounded between 1 and N_r, which is the maximum number of ring elements. For simplicity, in this paper we will always use the maximum number of ring elements ($K_{i+\frac{1}{2}} = N_r$). However we want to underline that in principle the semi-implicit 2D scheme allows to modify the number of active layers according to the wall deformation. The axial velocity u is located at the edge $x_{i+\frac{1}{2}}$

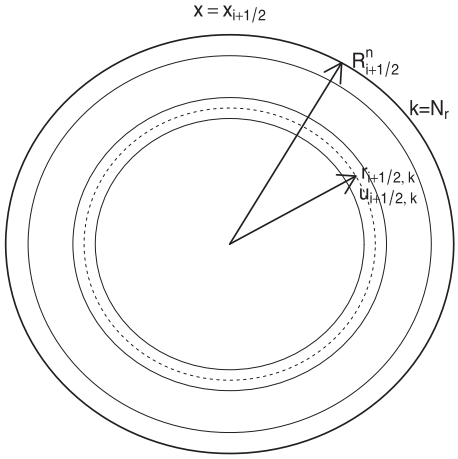

Fig. 2 Radial grid for the axial velocity u.

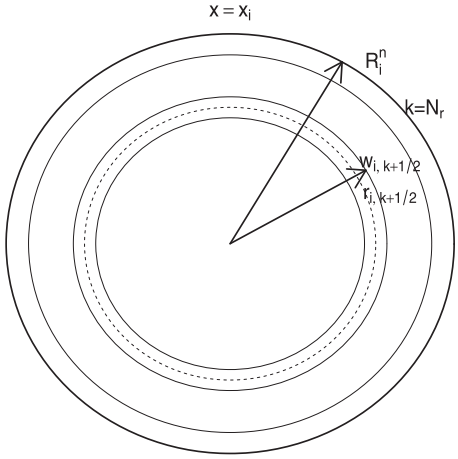

Fig. 3 Radial grid for the radial velocity w.

and at the midpoint $r_{i+\frac{1}{2},k}$ while $w_{i,k+\frac{1}{2}}$ is defined in the cell barycenter x_i and at the edge of the radial segment $r_{k+\frac{1}{2}}$ (see Figs. 2 and 3). This discretization of the computational domain yields again a staggered grid.

The momentum equation is discretized using a semi-implicit approach [14]:

$$\frac{q^{n+1}_{i+\frac{1}{2},k} - Fq^{n}_{i+\frac{1}{2},k}}{\Delta t} = -a^{n}_{i+\frac{1}{2},k}\frac{p^{n+\theta}_{i+1} - p^{n+\theta}_{i}}{\Delta x} + 2\pi\mu\left(r^{n}_{i+\frac{1}{2},k+\frac{1}{2}}\frac{u^{n+\theta}_{i+\frac{1}{2},k+1} - u^{n+\theta}_{i+\frac{1}{2},k}}{\Delta r^{n}_{i+\frac{1}{2},k+\frac{1}{2}}} - r^{n}_{i+\frac{1}{2},k-\frac{1}{2}}\frac{u^{n+\theta}_{i+\frac{1}{2},k} - u^{n+\theta}_{i+\frac{1}{2},k-1}}{\Delta r^{n}_{i+\frac{1}{2},k-\frac{1}{2}}}\right), \tag{30}$$

where $q^{n+1}_{i+\frac{1}{2},k} = \rho^{n}_{i+\frac{1}{2}} a^{n}_{i+\frac{1}{2}} u^{n+1}_{i+\frac{1}{2}}$ and $a^{n}_{i+\frac{1}{2},k} = 2\pi r^{n}_{i+\frac{1}{2},k}\Delta r^{n}_{i+\frac{1}{2}}$ are respectively the mass flow and the area of the k-th ring in position $x_{i+\frac{1}{2}}$. $Fq^{n}_{i+\frac{1}{2},k}$ is an explicit and non-linear operator for the convective terms. The discrete motion equation can be rewritten in a more compact form obtaining the vector of the mass fluxes [14]:

$$\mathbf{Q}^{\mathbf{n+1}}_{\mathbf{i+\frac{1}{2}}} = \left[\mathbf{D^{-1}G}\right]^{\mathbf{n}}_{\mathbf{i+\frac{1}{2}}} - \theta\frac{\Delta t}{\Delta x}\left(p^{n+1}_{i+1} - p^{n+1}_{i}\right)\left[\mathbf{D^{-1}A}\right]^{\mathbf{n}}_{\mathbf{i+\frac{1}{2}}}, \tag{31}$$

where $\mathbf{Q}^{\mathbf{n+1}}_{\mathbf{i+\frac{1}{2}}} = (q_{i+\frac{1}{2},1}, q_{i+\frac{1}{2},2}\dots q_{i+\frac{1}{2},K^n_{i+\frac{1}{2}}})^T$ and $\mathbf{A}^{\mathbf{n+1}}_{\mathbf{i+\frac{1}{2}}} = (a_{i+\frac{1}{2},1}, a_{i+\frac{1}{2},2}\dots a_{i+\frac{1}{2},K^n_{i+\frac{1}{2}}})^T$ are column vectors of the mass and of the area of the rings. $\mathbf{D}^{\mathbf{n}}_{\mathbf{i+\frac{1}{2}}}$ is a three-diagonal matrix which accounts for the coefficients of the viscous terms at the time $t^n + \Delta t$ (see [8, 14, 32]). The column vector $\mathbf{G}^{\mathbf{n}}_{\mathbf{i+\frac{1}{2}}}$ contains the non linear convective terms and the known quantities at time t^n. Eq. (29) is approximated by using a finite volume discretization. Also here the θ-method is used in order to improve time accuracy,

$$M\left(p^{n+1}_{i}\right) = M\left(p^{n}_{i}\right) - \Delta t\left(\mathbf{1^T}\cdot\mathbf{Q}^{\mathbf{n+\theta}}_{\mathbf{i+\frac{1}{2}}} - \mathbf{1^T}\cdot\mathbf{Q}^{\mathbf{n+\theta}}_{\mathbf{i-\frac{1}{2}}}\right), \tag{32}$$

where we have used the notation $\mathbf{1^T} = (1, 1, \cdots, 1)$ for a row vector consisting only of ones. Substituting the discrete momentum equation (31) into the discrete continuity equation Eq. (32), one obtains the following mildly non-linear system:

$$M\left(p^{n+1}_{i}\right) - \theta^2\frac{\Delta t^2}{\Delta x}\left\{\left(p^{n+1}_{i+1} - p^{n+1}_{i}\right)\left[\mathbf{1^T D^{-1}A}\right]^{\mathbf{n}}_{\mathbf{i+\frac{1}{2}}} - \left(p^{n+1}_{i} - p^{n+1}_{i-1}\right)\left[\mathbf{1^T D^{-1}A}\right]^{\mathbf{n}}_{\mathbf{i-\frac{1}{2}}}\right\} = b^{n}_{i}, \tag{33}$$

which has the same form of system (26) and is therefore solved in the same way at the aid of the (nested) Newton method. Once the pressure is known, the axial velocity is computed with Eq. (31), while the radial velocity is obtained from the discretization of the continuity equation (1). For more details about the numerical method, see [8, 14, 17, 32].

The stability condition of the semi-implicit schemes corresponds to the stability condition of the method used for the calculation of nonlinear convective terms. In general, the time step restriction is only based on the speed of the flow and *not* on the sound speed. Consequently, these schemes are very efficient, especially in the case of low Mach number flows. Moreover, if the convective terms can be neglected, one can simply set $Fq = q$, and in this case the schemes are *unconditionally stable*. However, the time step Δt should be chosen small enough to reduce the numerical viscosity and to resolve unsteady flow features properly.

In addition, it is rather simple to show that the semi-implicit schemes satisfy the so-called C-property, i.e. that these schemes are well-balanced. Consider the case where the cross sectional reference area of the pipe $A_0 = \pi R_0^2$ is not constant in longitudinal direction, while the pressure is constant ($p_i^n = \text{const}$) and the velocity is zero everywhere ($U_{i+\frac{1}{2}}^n = 0$). In this case the discrete pressure gradients in (20) are zero and also the non-linear convective terms are zero, which can be easily seen by inserting $U_{i+\frac{1}{2}}^n = 0$ into Eq. (21). Furthermore, also the unsteady friction terms vanish. As a result, the discrete mass fluxes $Q_{i+\frac{1}{2}}^{n+1} = 0$ at time t^{n+1} remain zero and thus the pressure remains unchanged ($p_i^{n+1} = p_i^n = \text{const}$), i.e. the steady state solution is exactly preserved.

2.3 Unsteady friction models

2.3.1 Convolution integral methods (CI)

The analytic expression for the calculation of the unsteady loss is given by the convolution integral of Zielke, see [41],

$$\tau_u(x,t) = \frac{2\mu}{R}\int_0^t \mathcal{W}(t-t^*)\frac{\partial U(x,t^*)}{\partial t}dt^*, \tag{34}$$

which is also called *frequency dependent friction*, since Zielke derived this expression in the complex domain after applying the Laplace transform. Moreover, he assumed incompressible and laminar flow in a rigid pipe and implemented his formula with the method of characteristics. In Eq. (34) the acceleration is multiplied by a weighting function $\mathcal{W}$ of the following form

$$\mathcal{W}(\hat{t}) = \begin{cases} \displaystyle\sum_{j=1}^{j=6} m_j \hat{t}^{0.5(j-2)} & \text{for} \quad \hat{t} \le 0.02, \\ \displaystyle\sum_{j=1}^{j=5} \mathrm{e}^{-n_j \hat{t}} & \text{for} \quad \hat{t} \ge 0.02, \end{cases} \tag{35}$$

where the coefficients are given by $(m_1, \ldots, m_6) = (0.282095, -1.250000, 1.057855, 0.937500, 0.396696, -0.351563)$ and $(n_1, \ldots, n_5) = (26.3744, 70.8493, 135.0198, 218.9216, 322.5544)$, while $\hat{t} = \nu t/R^2$ is the dimensionless time. Note that the domain of definition of the weighting function is $0 < \hat{t} < \infty$. The numerical evaluation of the convolution integral needs a very large memory amount and makes this approach computationally very expensive. Consequently, another more efficient approach is necessary. First, Trikha proposed in [34] an approximated weighting function of the following form:

$$\mathcal{W}_{app}(\hat{t}) = \sum_{j=1}^{N_w} m_j \mathrm{e}^{-n_j \hat{t}}, \tag{36}$$

with $N_w = 3$, $(m_1, m_2, m_3) = (40.0, 8.1, 1)$ and $(n_1, n_2, n_3) = (8000, 200, 26.4)$. Using a weighting function written as series of exponential functions, the unsteady wall shear is calculated with the formula of Trikha [34]

$$\tau_u^n \approx \frac{2\mu}{R}\sum_{j=1}^{3} y_j^n = \frac{2\mu}{R}\left(\sum_{j=1}^{3} \mathrm{e}^{-n_j \frac{\nu\Delta t}{R^2}} y_j^{n-1} + \sum_{j=1}^{3} m_j \left[U^n - U^{n-1}\right]\right), \tag{37}$$

which improved the efficiency but not the accuracy because the weighting function of Trikha does note reproduce well the original function. Successively Kagawa et al. [21] proposed a more accurate weighting function with $N_w = 10$ terms (valid for $6.31 \cdot 10^{-6} \le \hat{t} < \infty$) and another formula to approximate the Zielke convolution integral:

$$\tau_u^n \approx \frac{2\mu}{R}\sum_{j=1}^{N_w} y_j^n = \frac{2\mu}{R}\left(\sum_{j=1}^{N_w} \mathrm{e}^{-n_j \frac{\nu\Delta t}{R^2}} y_j^{n-1} + \sum_{j=1}^{N_w} m_j \mathrm{e}^{-n_j \frac{\nu\Delta t}{2R^2}} \left[U^n - U^{n-1}\right]\right). \tag{38}$$

The coefficients of the Kagawa weighting function are $(n_1, \ldots, n_{10}) = (26.3744, 72.8033, 187.424, 536.626, 1570.60, 4618.13, 13601.1, 40082.5, 118153, 348316)$ and $(m_1, \ldots, m_{10}) = (1, 1.16725, 2.20064, 3.92861, 6.78788, 11.6761, 20.0612, 34.4541, 59.4541, 101.59)$.

Other authors proposed other values for the coefficients m_j and n_j for the approximated weighting function Eq. (36), such as Vitkovsky et al. [39] and Vardy and Brown [38]. In addition, Urbanowicz and Zarzycky [35] recently proposed a very accurate function with $N_w = 26$, defined in the range $10^{-9} \le \hat{t} < \infty$: $(n_1, \ldots, n_{26}) = (26.3744, 70.8493,$

135.0198, 218.9216, 322.5544, 499.148, 1072.543, 2663.013, 6566.001, 15410.459, 35414.779, 80188.189, 177078.960, 388697.936, 850530.325, 1835847.582, 3977177.832, 8721494.927, 19120835.527, 42098544.588, 92940512.285, 203458923, 445270063.893, 985067938, 2166385707.058, 4766167206.672) and $(m_1, \ldots, m_{26}) = (1, 1, 1, 1, 1, 2.141, 4.544, 7.566, 11.299, 16.531, 24.794, 36.229, 52.576, 78.150, 113.873, 165.353, 247.915, 369.561, 546.456, 818.871, 1209.771, 1770.756, 2651.257, 3968.686, 5789.566, 8949.468)$. For a very nice review of convolution integral theory and of its approximation see [35].

2.3.2 Instantaneous acceleration methods (IA)

Another class of unsteady friction models is the one called Instantaneous Acceleration based models and is based on the hypothesis that the unsteady wall shear stress is directly proportional to the acceleration of the flow. To the knowledge of the authors, the most complete model of this family is the one of Brunone et al. which is formulated as follows [3,4,28]:

$$\tau_{us} = \frac{\rho D K_{Bru}}{4}\left(\frac{\partial U}{\partial t} + \text{sign}\left(U\frac{\partial U}{\partial x}\right)c_0\frac{\partial U}{\partial x}\right). \tag{39}$$

Several values have been proposed for the coefficient K_{Bru} and in this paper we use the expression suggested by Vardy and Brown in [37] because it seems to be the only one related to the Reynolds number

$$K_{Bru} = 2\sqrt{\frac{7.41}{\text{Re}^{\chi}}}, \quad \chi = \log\left(\frac{14.3}{\text{Re}^{0.05}}\right). \tag{40}$$

2.4 A new efficient approximation of the Zielke convolution integral

The numerical integration of a convolution integral can be very computationally expensive, especially when long time simulations are required. Here, we derive a new simplification of the model of Zielke that leads to a new efficient formula for the evaluation of the unsteady wall shear stress. This approach takes follows the approach used in the work of Moczo and Kristek that simplified convolution integrals in order to compute efficiently material-independent anelastic functions for seismic wave propagation [24]. Substituting a weighting function expressed as a sum of exponential functions (Eq. (36)) into the convolution integral, the total wall shear is computed as $\tau_u = \sum_j^{N_w} \tau_j$, where the j-th component is written as follows

$$\tau_j(t) = \frac{2\mu}{R}\int_0^t m_j \mathrm{e}^{-\frac{n_j \nu}{R^2}(t-t^*)}\frac{dU(t^*)}{dt}dt^*. \tag{41}$$

The coefficients m_j and n_j can be taken from any of the approximated weighting functions previously cited. Deriving with respect to time the left and the right side of the previous equation and applying the Leibniz rule, we obtain the expression

$$\frac{d}{dt}\tau_j(t) = -\frac{2\mu}{R}\int_0^t \frac{dU(t^*)}{dt} m_j \frac{n_j \nu}{R^2}\mathrm{e}^{-\frac{n_j \nu}{R^2}(t-t^*)}dt^* + \frac{2\mu}{R}\frac{dU(t)}{dt}m_j \tag{42}$$

that can be formally rewritten as an ordinary differential equation

$$\frac{d}{dt}\tau_j(t) = -\frac{n_j \nu}{R^2}\tau_j + \frac{2\mu}{R}\frac{dU(t)}{dt}m_j. \tag{43}$$

Since the coefficients n_j can assume very large values [21,35,38,39], the source terms in the ODE (43) are stiff. Hence, for efficiency and stability reasons, the ODE (43) is approximated by using the *implicit* Euler method

$$\frac{\tau_j^n - \tau_j^{n-1}}{\Delta t} = -\frac{n_j \nu}{R^2}\tau_j^n + \frac{2\mu}{R}\frac{U^n - U^{n-1}}{\Delta t}m_j, \tag{44}$$

and finally, after solving for the quantity τ_j^n, the unsteady friction term at time t^n reads:

$$\tau_u^n = \sum_{j=1}^{N_w}\tau_j^n = \sum_{j=1}^{N_w}\frac{\tau_j^{n-1} + \frac{2\mu}{R}m_j(U^n - U^{n-1})}{1 + \frac{n_j \nu}{R^2}\Delta t}. \tag{45}$$

Here, we deliberately omit the spatial index for the averaged velocity U, since the above formula (45) applies to both, the path-conservative finite volume scheme on collocated grids, as well as to the semi-implicit finite volume method on staggered grids.

3 Numerical results

In this section we show and compare the computational results that have been obtained by applying the previously presented numerical schemes. We use some abbreviations: PC1D for the explicit path conservative scheme applied to the 1D model, SI1D and SI2D for the semi-implicit schemes applied to the one-dimensional and to the two dimensional PDE, respectively. The unsteady friction model of Urbanowicz and Zarzycki is abbreviated by UZ model. Furthermore, Kagawa ODE and UZ ODE indicate that the new approximation of the Zielke convolution integral based on the ODE solver (45) that has been implemented by using the coefficients of the weighting function of Kagawa et al. [21] and of Urbanowicz and Zarzycky [35], respectively. In addition, the Osher Riemann solver and the HLL Riemann solver give very similar results for the 1D PDE system, which can be explained by the fact that the system does not contain any linearly degenerate intermediate field. Consequently, in the next plots the numerical solution for the explicit path-conservative finite volume scheme is referred to the one computed by using the Osher Riemann solver, in order to keep the images clear and readable. The differences between the methods can be appreciated in terms of accuracy and computational time for the simulations.

3.1 Womersley test

For the first test considered the fluid is assumed incompressible ($c_0 = 10^{20}$) and the pipe rigid ($E_\infty = 10^{20}$). Consequently, this test case can be numerically performed only by using the semi-implicit schemes because when the speed of sound c_0 and thus also the the maximum eigenvalue ($\max|\mathbf{\Lambda}(\mathbf{Q}_\mathbf{i}^\mathbf{n})|$) tends to infinity, the system (1) is no longer hyperbolic.

An oscillating pressure gradient of the following form

$$p_{in}(t) = \Re(p_{out} + LA_w e^{j\omega t}) = p_{out} + LA_w \cos(\omega t) \tag{46}$$

is imposed in a pipe of length L and radius R. The pressure wave is characterized by an amplitude A_w and by an angular frequency $\omega = 2\pi f$. Due to the incompressibility and rigidity conditions, the pressure varies linearly along the longitudinal coordinates. The axial velocity u is constant in longitudinal direction while the radial profile is given by the analytic solution of Womersley [40]

$$u(r,t) = \Re\left\{ A_w \frac{1}{j\omega}\left[1 - \frac{J_o(\hat{r} j^{3/2}\mathrm{Wo})}{J_o(j^{3/2}\mathrm{Wo})}\right] e^{j\omega t}\right\}, \tag{47}$$

where $j = \sqrt{-1}$ is the imaginary unit, $\mathrm{Wo} = R\sqrt{\frac{\omega}{\nu}}$ denotes the Womersley number and J_o is the zero-th order Bessel function of complex argument.

For this test we consider $L = 1$ m, $R = 4 \cdot 10^{-3}$ m, $p_{out} = 5 \cdot 10^5$ Pa, $A_w = 1000$ Pa, $f = 500$ Hz, and $\rho_0 = 998.2$ kg/m^3. According to the solution derived by Womersley, the convective terms are neglected. The numerical parameter for the grids are $N_x = 500$ and $N_r = 50$ while the time step has been imposed as $\Delta t = f^{-1}/100$ hence a single wave period is resolved in 100 time steps (100 points per wave length). As initial conditions, in the code for the semi-implicit two dimensional method we imposed the velocity profile given by $u(r,0)$ while for the one dimensional semi-implicit method, the mean velocity is equal to $U = 1/A \int u(r,0) dA$.

The velocity computed by the scheme SI2D has to be cross-sectionally averaged in order to have a consistent comparison against the velocity given by averaged SI1D method, for which we have implemented and tested several unsteady friction models. Similarly, also the exact solution in Eq. (47) is averaged over the cross section, in order to have the exact mean velocity that is subsequently compared against all numerical results.

First, a dynamic viscosity of $\mu = 10^{-3}$ Pa·s is chosen. In Figs. 4–7 the reference solution is well fitted by the numerical solution of SI2D but also by all the friction models implemented in SI1D. Later on, the viscosity has been increased by three order of magnitude, hence $\mu = 1$ Pa·s. In this case, the exact solution is well fitted by all friction models, apart from the models of Trikha and Brunone, see Fig. 9. The first disagreement could be justified by the fact that Trikha's weighting function doesn't approximate well the original function of Zielke. The second mismatch could be explained because the Brunone model does not take into account the past acceleration of the flows, such as the model of Zielke and, consequently, also all its approximations.

3.2 Impedance matrix for weakly compressible flow in the frequency domain

The next investigation regards the comparison of the numerical solutions against an analytic solution derived in the frequency domain that is valid for weakly compressible laminar flows and which has been exposed in [23]. The system of Eqs. (27) is simplified neglecting the radial velocity w and the convective terms of the momentum equations. Further assumption is the hypothesis of periodic laminar flow in a situation such that the friction effects given by the frequency are

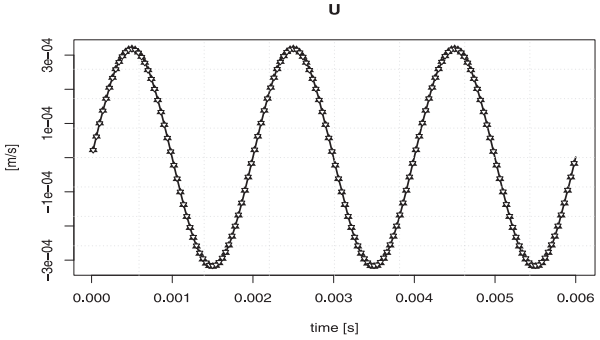

Fig. 4 Womersley test, $\mu = 10^{-3}$. Exact solution (—), numerical data given by SI2D (▲) and by SI1D with Zielke model (▽).

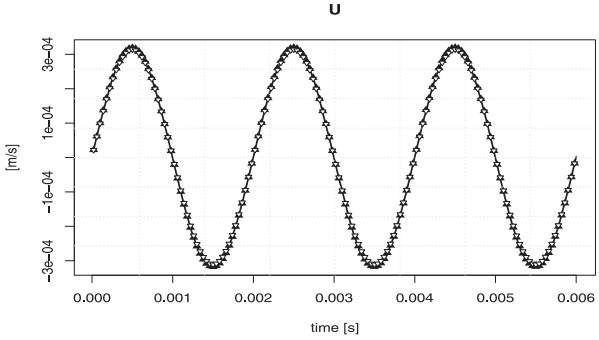

Fig. 5 Womersley test, $\mu = 10^{-3}$. Exact solution (—), numerical data given by SI1D with Trikha model (▲) and with Brunone model (▽).

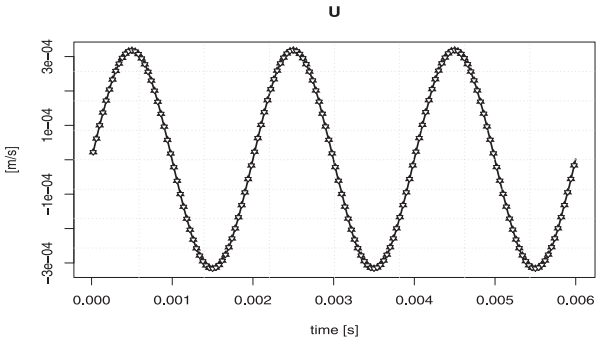

Fig. 6 Womersley test, $\mu = 10^{-3}$. Exact solution (—), numerical data given by SI1D with Kagawa model (▲) and with Kagawa ODE model (▽).

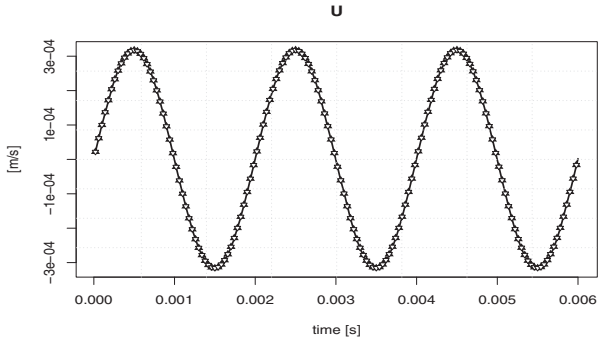

Fig. 7 Womersley test, $\mu = 10^{-3}$. Exact solution (—), numerical data given by SI1D with UZ model (▲) and with UZ ODE model (▽).

higher than those of quasi-steady flow conditions. Applying the Laplace transform one obtains the following expression for an hydraulic system composed by a tube of length L and radius R

$$\begin{bmatrix} \hat{p}_1(s) \\ \hat{p}_2(s) \end{bmatrix} = \mathbf{Z}(\mathbf{s}) \begin{bmatrix} \hat{Q}_1(s) \\ \hat{Q}_2(s) \end{bmatrix} = \begin{bmatrix} Z_L(s)\frac{\cosh(\gamma(s)L)}{\sinh\gamma(s)L} & -Z_L(s)\frac{1}{\sinh(\gamma(s)L)} \\ Z_L(s)\frac{1}{\sinh(\gamma(s)L)} & -Z_L(s)\frac{\cosh(\gamma(s)L)}{\sinh\gamma(s)L} \end{bmatrix} \begin{bmatrix} \hat{Q}_1(s) \\ \hat{Q}_2(s) \end{bmatrix}, \tag{48}$$

where $s = jw$ is the Laplace parameter, $\hat{p}(x,s)$ and $\hat{Q}(x,s)$ are the complex pressure and the complex volume flow rate. The indices 1 and 2 denote the quantities at the inlet and at the outlet of the tube, respectively. Consequently, we have $\hat{p}_1 = \hat{p}(0,s)$, $\hat{p}_2 = \hat{p}(L,s)$, and $\hat{Q}_1 = \hat{Q}(0,s)$, and $\hat{Q}_2 = \hat{Q}(L,s)$. $\mathbf{Z}(\mathbf{s})$ is the impedance matrix and its elements are expressed as functions of the hyperbolic sinus and cosine functions. Moreover, Z_L is a transfer coefficient given by

$$Z_L(s) = Z_0\sqrt{\frac{J_0(R^*)}{J_1(R^*)}} \quad \text{with} \quad Z_0 = \frac{\sqrt{E'\rho}}{\pi R^2}, \quad E' = E\frac{1}{1+\frac{E}{E_\infty}W}, \tag{49}$$

where Z_0 is the frictionless case of Z_L and E' is the modified total bulk modulus of the system that takes into account also the wall elasticity. Here, E_∞ is the Young modulus of the wall material and E is the bulk modulus of the fluid, commonly defined as $E = \rho_0 c_0^2$; γ is a wave propagation parameter that is essentially a function of the speed of sound and of the complex radius R^*:

$$\gamma(s) = \frac{s}{c_0}\sqrt{-\frac{J_0(R^*)}{J_2(R^*)}} \quad \text{with} \quad R^* = j\sqrt{\frac{s}{\nu}}R. \tag{50}$$

In order to compute the elements of the impedance matrix for a numerical simulation in the time domain, a frequency has to be fixed and then an oscillatory pressure gradient is imposed, exactly like in the Womersley test. The complex quantities $\hat{p}$ and $\hat{Q}$ are then computed by applying the fast Fourier transformation to the time signals of the numerical pressure and mass flow rates taken at the inlet and at the outlet of the tube. Applying an oscillating pressure signal of the same form

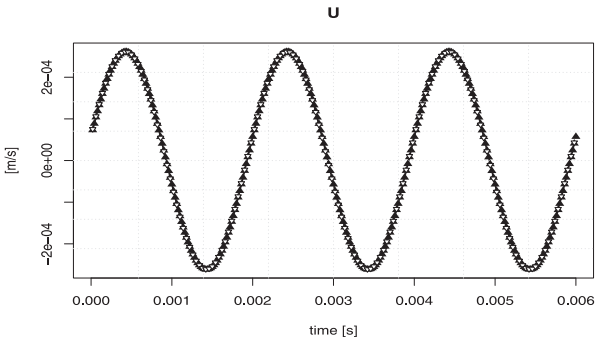

Fig. 8 Womersley test, $\mu = 1$. Exact solution (—), numerical data given by SI2D (▲) and by SI1D with Zielke model (▽).

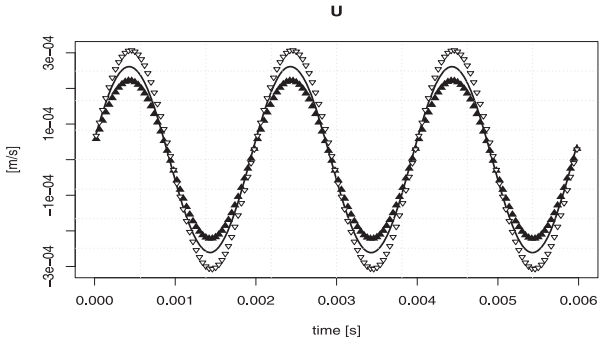

Fig. 9 Womersley test, $\mu = 1$. Exact solution (—), numerical data given by SI1D with Trikha model (▲) and with Brunone model (▽).

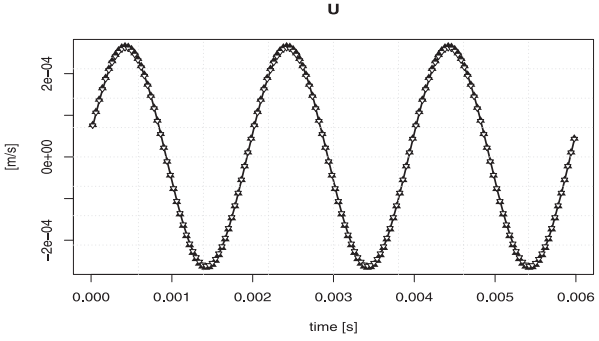

Fig. 10 Womersley test, $\mu = 1$. Exact solution (—), numerical data given by SI1D with Kagawa model (▲) and with Kagawa ODE model (▽).

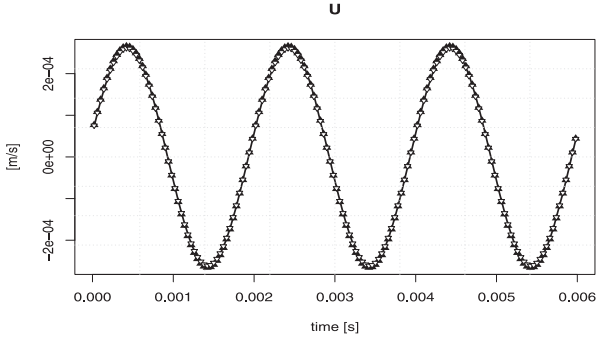

Fig. 11 Womersley test, $\mu = 1$. Exact solution (—), numerical data given by SI1D with UZ model (▲) and with UZ ODE model (▽).

given by Eq. (46) the complex pressure at the outlet $\hat{p}_2$ is much smaller than the complex pressure at the inlet of the pipe $\hat{p}_1$. Moreover, it is possible to demonstrate that the impedance matrix is symmetric and consequently the elements z_{11} and z_{12} of the impedance matrix can be computed as follows [18, 23]:

$$z_{11}(s) = \frac{\hat{p}_1(s)\hat{Q}_1(s)}{\hat{Q}_1^2(s) - \hat{Q}_2^2(s)}, \quad z_{12}(s) = -\frac{\hat{p}_1(s)\hat{Q}_2(s)}{\hat{Q}_1^2(s) - \hat{Q}_2^2(s)}. \tag{51}$$

For additional details about the impedance theory see [23].

3.2.1 Rigid case

First, the numerical models are applied in order to reproduce existing experimental measurements that have been obtained for a test fluid in a rigid pipe characterized by radius $R = 4$ mm and length $L = 0.791$ m. In the semi-implicit schemes the longitudinal resolution is equal to 1 mm and consequently the number of cells is 791. The radial grid for SI2D is composed by 50 equally spaced layers. On the contrary, for the path conservative method the number of cells N_x has been chosen equal to 395 that gives a resolution of 2 mm. This choice for the parameters Δx and Δt comes from the result of a series of preliminary simulations that will be discussed in Subsect. 3.4. The investigated frequency range goes from 50 Hz to 2000 Hz using a frequency step of 10 Hz. In addition, both in the numerical simulations as well as in the measured data, a transient phase occurs at the beginning of the experiments. During this period the mass flow signals are not regular, but experiences have shown that they becomes cleaner after 0.1 s. Moreover, the fast Fourier transform has been applied to the signal composed by the last 50 wave periods. Consequently, for each frequency the final time of the simulation is equal to $0.1 + 50/f$. According to the hypothesis of this theory the convective terms are neglected and the semi-implicit schemes are unconditionally stable but, in order to limit the numerical viscosity and to resolve the unsteady flow features properly, the parameter Δt is imposed equal to $T_w/100$, where T_w is the wave period ($T_w = f^{-1}$).

In Fig. 12 one can see that the numerical solution of the scheme SI2D reproduces perfectly well the analytic solution without the use of any friction model, since the 2D model is based on first principles and directly discretizes the viscous

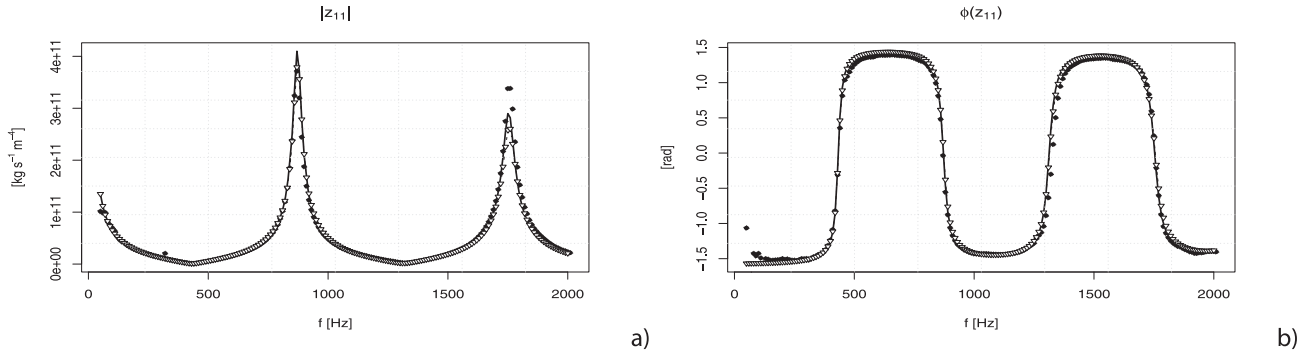

a) b)

Fig. 12 Absolute value and phase of the element z_{11} of the impedance matrix for a test fluid in a rigid pipe - Reference solution (——), experimental data (•) and numerical data from the method SI2D ▲.

terms from the available radial velocity profiles. In Fig. 13 the first element of the impedance matrix is computed using the one dimensional schemes PC1D and SI1D without any unsteady friction model; here, the numerical data do not fit the exact solution and, consequently it is possible to understand the crucial role of unsteady (frequency-dependent) friction models. According to the results of the previous test, also in this case the approximations proposed by Trikha (see Fig. 14) and the model of Brunone (see Fig. 19) do not give good agreements with the reference solution. In the next four figures (Figs. 15–18) the coefficients of the weighting functions of Kagawa and of Urbanowicz and Zarzycky are used to compute the contribution of the unsteady wall shear stress by using both the formula of Kagawa (Eq. 38) and the new ODE integrator (Eq. 45); in all these cases the agreement is very good.

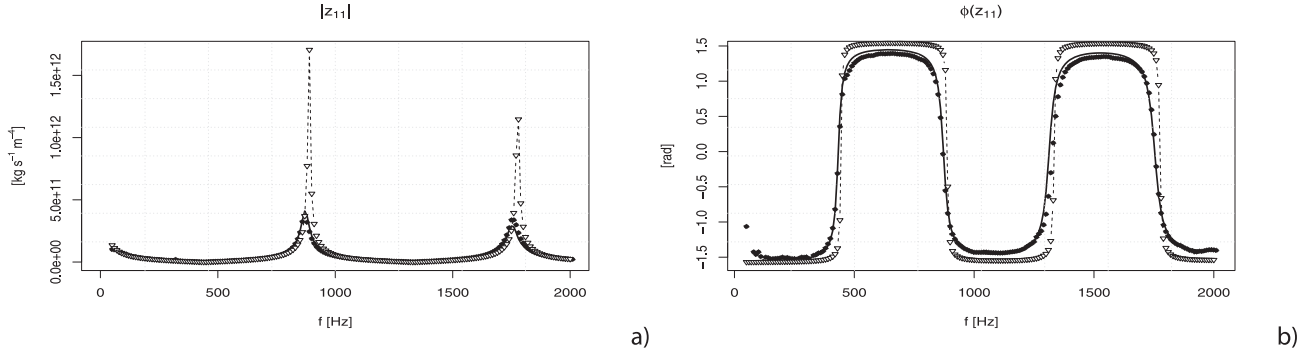

a) b)

Fig. 13 Absolute value and phase of the element z_{11} of the impedance matrix for a test fluid in a rigid pipe - Reference solution (——), experimental data (•) and numerical data from the method SI1D (▲) and from PC1D (▽) using only a steady friction model.

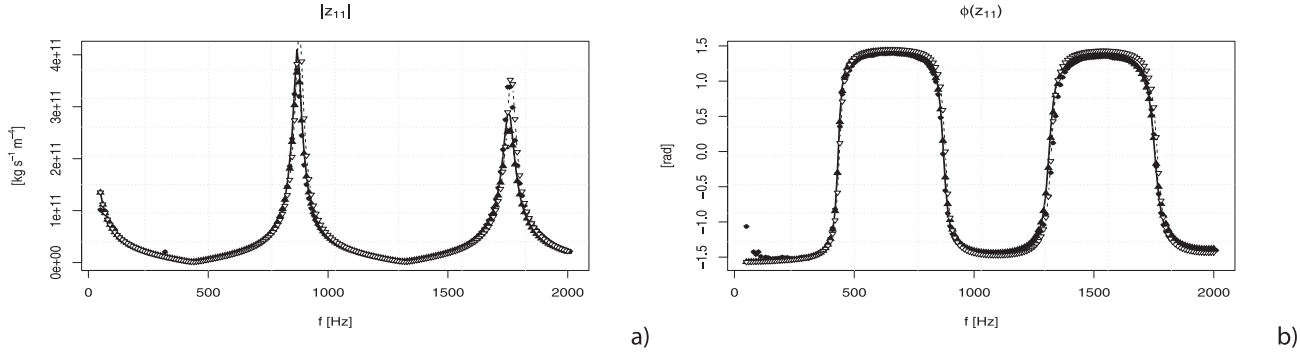

a) b)

Fig. 14 Absolute value and phase of the element z_{11} of the impedance matrix for a test fluid in a rigid pipe - Reference solution (——), experimental data (•) and numerical data from the method SI1D (▲) and from PC1D (▽) with Trikha model for the unsteady friction term.

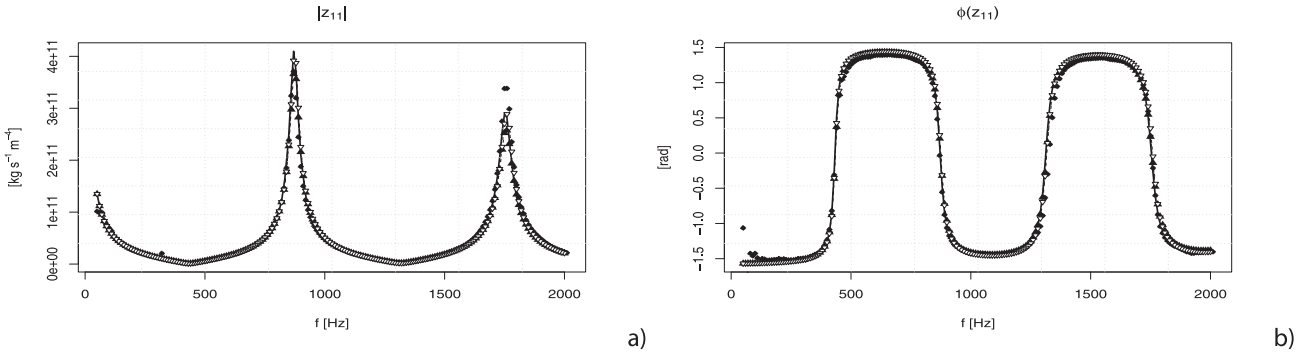

Fig. 15 Absolute value and phase of the element z_{11} of the impedance matrix for a test fluid in a rigid pipe - Reference solution (——), experimental data (•) and numerical data from the method SI1D (▲) and from PC1D (▽) with Kagawa model for the unsteady friction term.

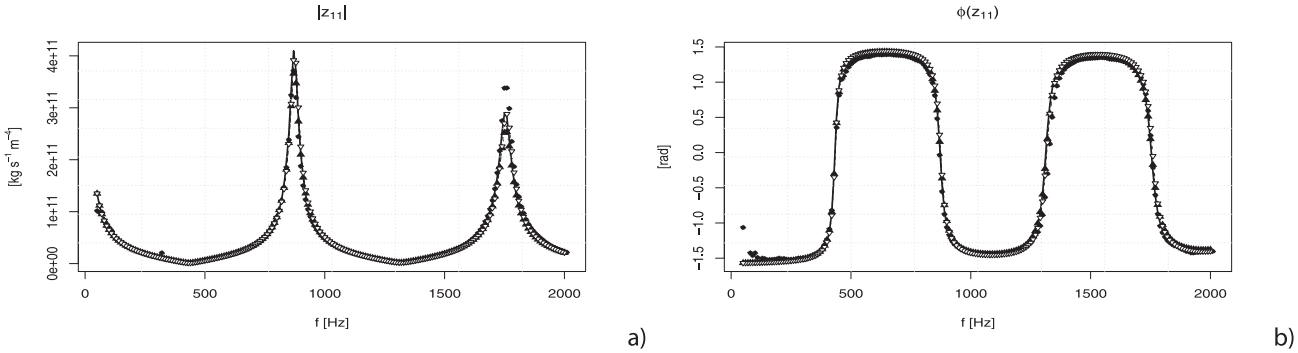

Fig. 16 Absolute value and phase of the element z_{11} of the impedance matrix for a test fluid in a rigid pipe - Reference solution (——), experimental data (•) and numerical data from the method SI1D (▲) and from PC1D (▽) with Kagawa ODE model for the unsteady friction term.

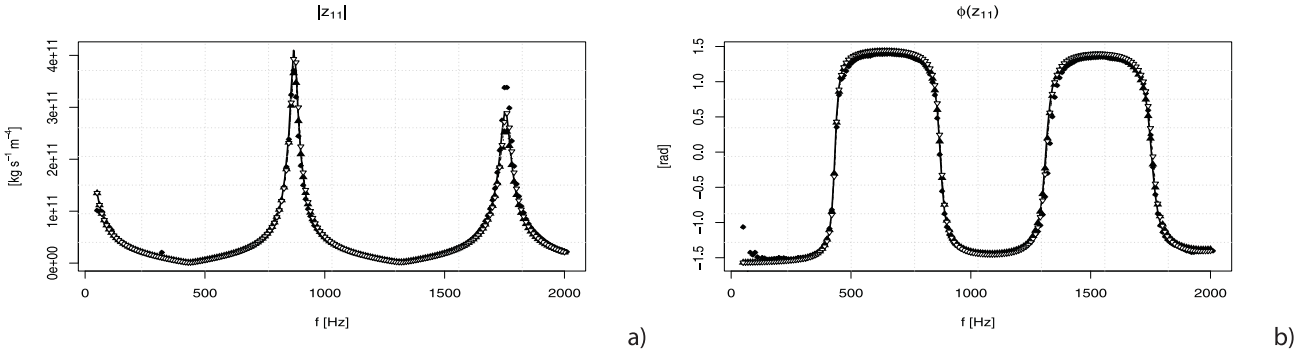

Fig. 17 Absolute value and phase of the element z_{11} of the impedance matrix for a test fluid in a rigid pipe - Reference solution (——), experimental data (•) and numerical data from the method SI1D (▲) and from PC1D (▽) with Urbanowicz and Zarzycky model for the unsteady friction term.

3.2.2 Elastic case

Second, the frequency domain is investigated for a generic fluid in a flexible pipe. The wall deformation is governed by the Hooke law presented at the beginning of this paper. It is a very simple model for the tube wall and for comparison against experimental data more sophisticated equations must be used. However, the advantage of the Hooke model used for these simulations is that it can be easily taken into account in the exact solution of the impedance matrix. The fluid properties are: $\rho_0 = 998.2$ kg/m^3, $c_0 = 1400$ m/s, and $\mu = 10^{-2}$ Pa·s. The length of the pipe is $L = 1$ m and the radius $R = 1$ mm while the Young's modulus is $E_\infty = 1 \cdot 10^{10}$ Pa. The longitudinal resolution is still 1 mm for the semi-implicit schemes while it is equal to 2 mm for the path conservative method. The other numerical parameters are taken equal to the case of the rigid pipe. The semi-implicit 2D model gives again a very good match compared against the reference solution (see Fig. 20) and also for this test when the unsteady friction is neglected in the 1D models the disagreement remains

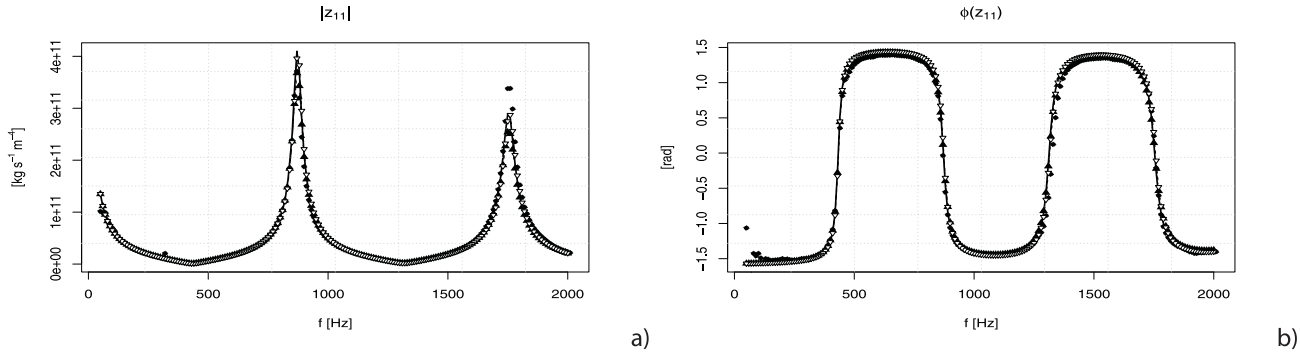

Fig. 18 Absolute value and phase of the element z_{11} of the impedance matrix for a test fluid in a rigid pipe - Reference solution (———), experimental data (•) and numerical data from the method SI1D (▲) and from PC1D (▽) with Urbanowicz and Zarzycky ODE model for the unsteady friction term.

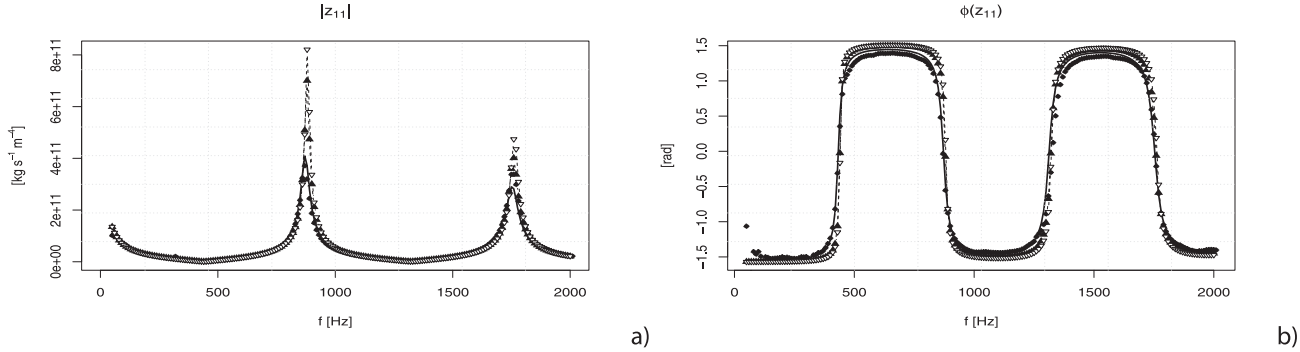

Fig. 19 Absolute value and phase of the element z_{11} of the impedance matrix for a test fluid in a rigid pipe - Reference solution (———), experimental data (•) and numerical data from the method SI1D (▲) and from PC1D (▽) with Brunone model for the unsteady friction term.

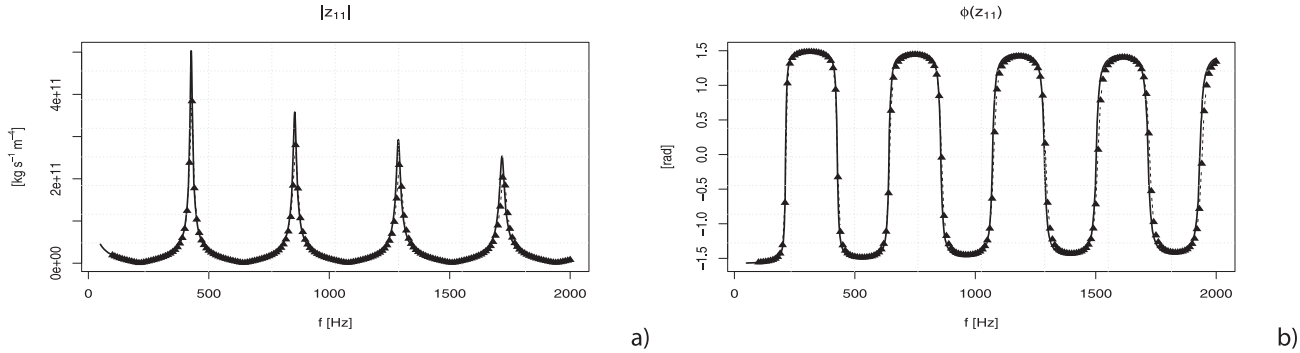

Fig. 20 Absolute value and phase of the element z_{11} of the impedance matrix for a compressible fluid in an elastic pipe - Reference solution (———) and numerical data from the method SI2D ▲.

high (see Fig. 21). The 1D schemes implemented accounting for the unsteady friction via the convolution integral family match very well the reference solution in the frequency domain (see Figs. 22–26). Also the Trikha method works well (see Fig. 22) because the viscosity of the fluid is quite small. However, as shown in Fig. 27, the model of Brunone still gives significant disagreements when compared against the exact solution in the frequency domain. We want to underline that the approximations of the Zielke model fit the analytic solution for compressible flow in elastic ducts very well, although the original model was proposed for *incompressible* fluids in *rigid* pipes! Moreover, for these tests the simulations are very long and it is practically impossible to get the results by using the original Zielke method due to its slowness and due to the massive memory amount that it requires.

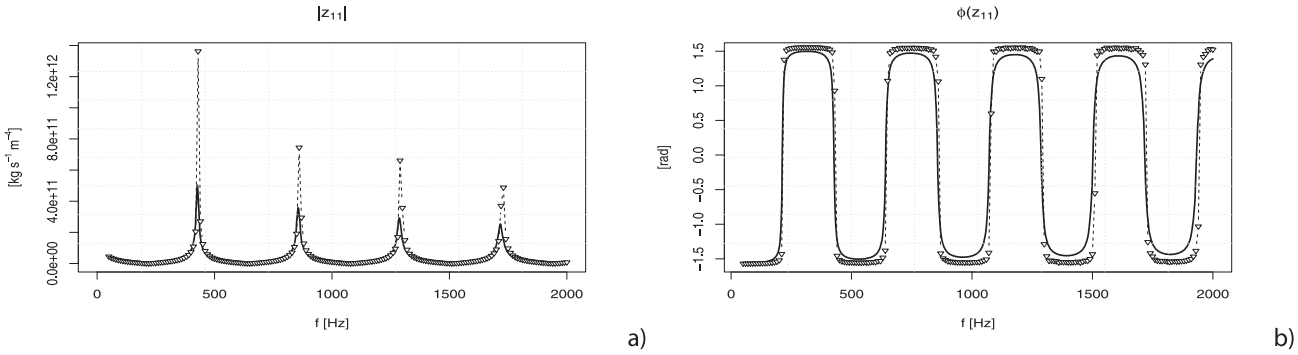

Fig. 21 Absolute value and phase of the element z_{11} of the impedance matrix for a compressible fluid in an elastic pipe - Reference solution (——) and numerical data from the method SI1D (▲) and from PC1D (▽) accounting only the steady friction term.

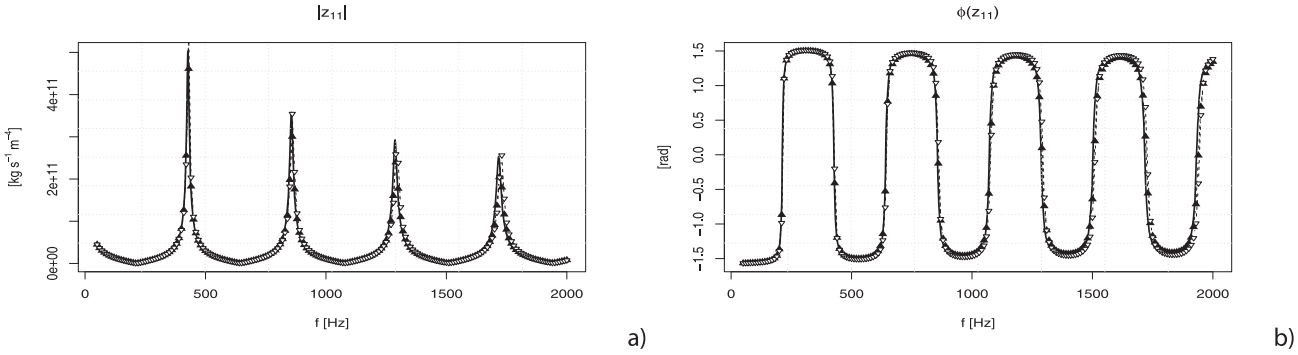

Fig. 22 Absolute value and phase of the element z_{11} of the impedance matrix for a compressible fluid in an elastic pipe - Reference solution (——) and numerical data from the method SI1D (▲) and from PC1D (▽) with Trikha model for the unsteady friction term.

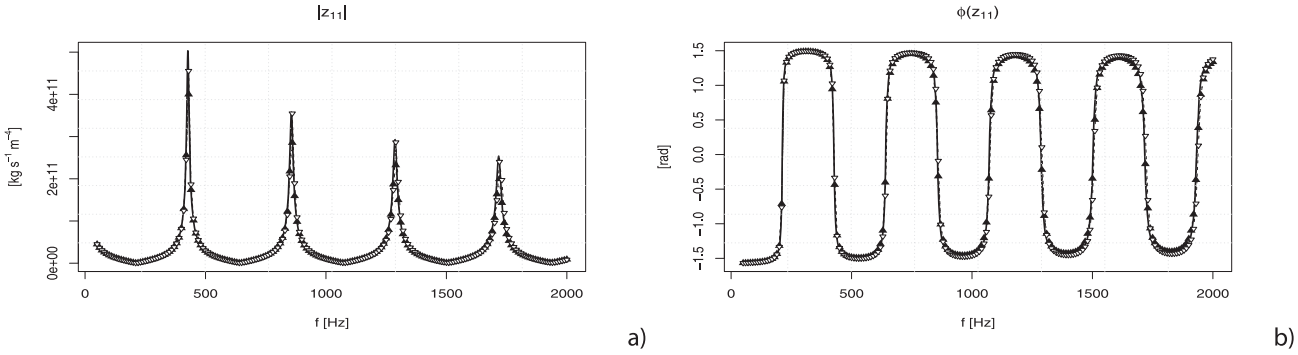

Fig. 23 Absolute value and phase of the element z_{11} of the impedance matrix for a compressible fluid in an elastic pipe - Reference solution (——) and numerical data from the method SI1D (▲) and from PC1D (▽) with Kagawa model for the unsteady friction term.

3.3 Water hammer

The last test presented in this paper is a typical benchmark problem used to assess the quality of different unsteady friction models. In a long pipeline characterized by normal flow and with an upstream constant hydraulic head given for example by a reservoir, the downstream valve is suddenly closed generating a pressure wave that travels back into the pipe and then it is periodically reflected. This is known as the experiment of Holmboe and Rouleau [20] and from their results it was understood that the unsteady friction contribution is crucial in order to predict the pressure damping at the downstream border of the pipe correctly. Here, we consider a fluid which has similar physical properties of water: $\rho_0 = 998.2$ kg/m^3, $c_0 = 1400$ m/s, $\mu = 10^{-3}$ Pa·s. The length of the pipe is $L = 15$ m and the radius is $R = 4$ mm. For all the schemes the number of cells is $N_x = 1000$, because we decided to take the pressure signals in the same position in order to compare the numerical data in the best way possible. In addition, for SI2D the number of rings is $N_r = 50$ and for both the semi-implicit

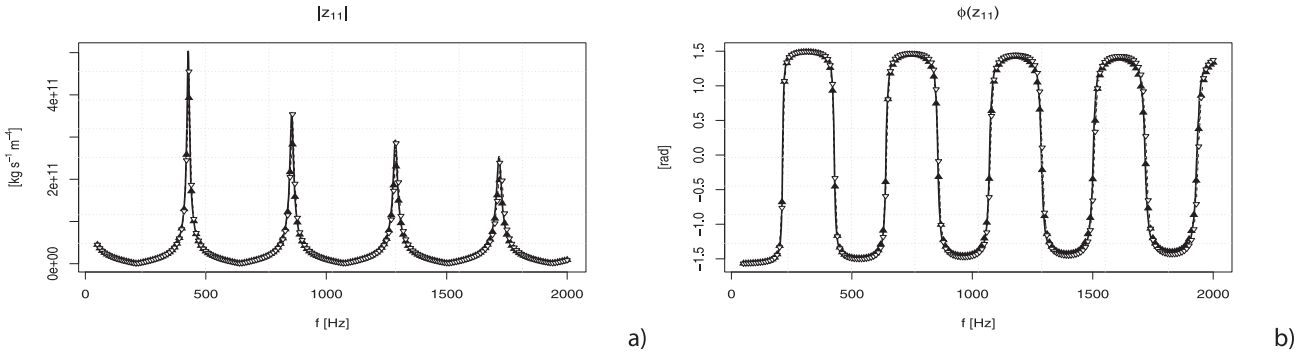

Fig. 24 Absolute value and phase of the element z_{11} of the impedance matrix for a compressible fluid in an elastic pipe - Reference solution (_____) and numerical data from the method SI1D (▲) and from PC1D (▽) with Kagawa ODE model for the unsteady friction term.

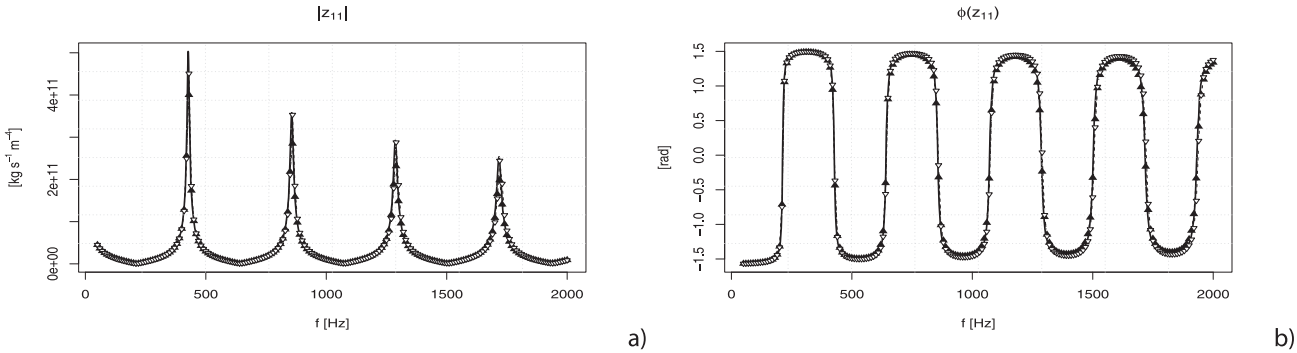

Fig. 25 Absolute value and phase of the element z_{11} of the impedance matrix for a compressible fluid in an elastic pipe - Reference solution (_____) and numerical data from the method SI1D (▲) and from PC1D (▽) with Urbanowicz and Zarzycky model for the unsteady friction term.

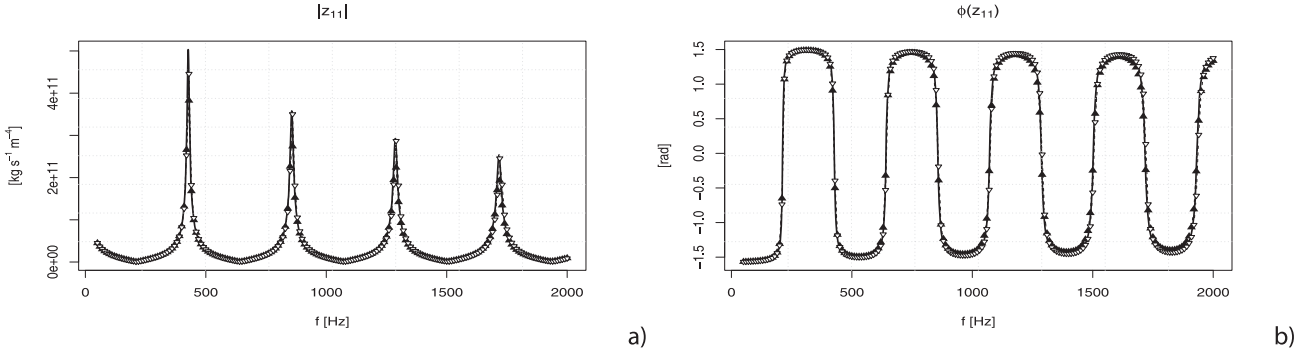

Fig. 26 Absolute value and phase of the element z_{11} of the impedance matrix for a compressible fluid in an elastic pipe - Reference solution (_____) and numerical data from the method SI1D (▲) and from PC1D (▽) with Urbanowicz and Zarzycky ODE model for the unsteady friction term.

schemes the time step Δt is imposed equal to $2 \cdot 10^{-5}$ s to reduce the numerical viscosity introduced by the implicit time discretization.

The aim of this analysis is to compare the behavior of the different unsteady friction models considered in this paper. We assume that the reference solution for the pressure at the end of the tube is the numerical one given by SI2D, since it is the only method that is able to evaluate the friction term directly from first principles, without any closure relation.

In Fig. 28 the results of the Trikha method implemented in SI1D and in PC1D are shown. It is possible to observe that both numerical schemes (SI1D and PC1D) give very similar results with the same unsteady friction model, which, however, deviate from the reference solution. In Fig. 29 the numerical data obtained from the Brunone model are exposed and a disagreement can be seen, but this behavior is intrinsic to the Brunone model and has been observed also by other authors, see for example [28].

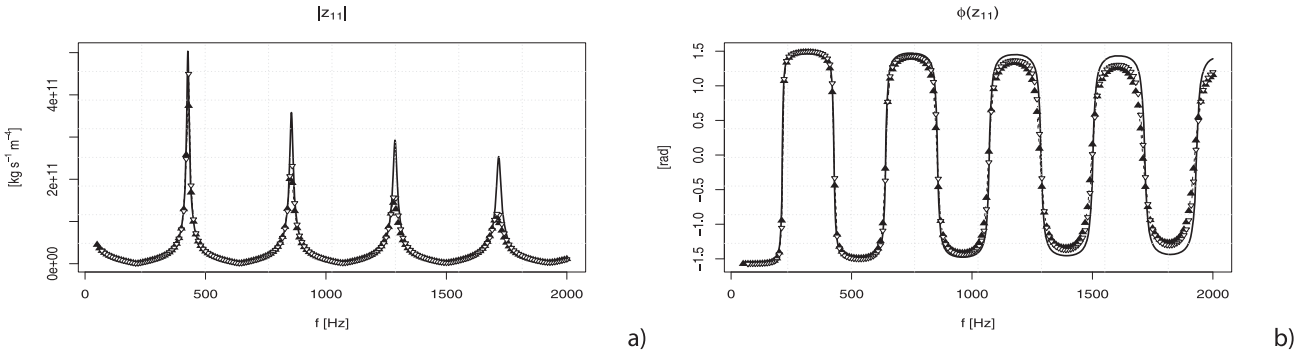

Fig. 27 Absolute value and phase of the element z_{11} of the impedance matrix for a compressible fluid in an elastic pipe - Reference solution (——) and numerical data from the method SI1D (▲) and from PC1D (▽) with Brunone model for the unsteady friction term.

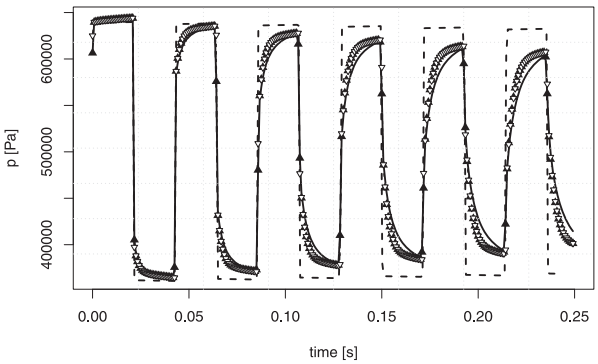

Fig. 28 Water hammer, rigid pipe - Reference solution (—), 1D methods without unsteady friction (- - -), numerical data given by SI1D with Trikha model (▲) and by PC1D with Trikha model (▽).

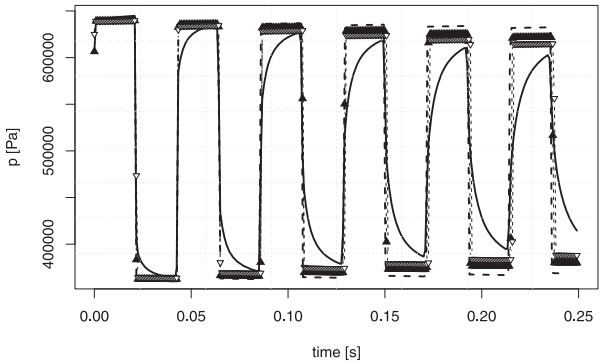

Fig. 29 Water hammer, rigid pipe - Reference solution (—), 1D methods without unsteady friction (- - -), numerical data given by SI1D with Brunone model (▲) and by PC1D with Brunone model (▽).

Fig. 30 and Fig. 31 show the results of the Kagawa coefficients used in the original formula of Kagawa (38) and in our new ODE method (45). The results illustrate a very good fitting with the reference solution. The same conclusion can be observed applying the UZ model coefficients, see Figs. 32 and 33.

As conclusive test, we repeat the previous simulations for an elastic tube with $E_\infty = 10^{10}$ Pa and with an increased viscosity equal to $\mu = 10^{-1}$ Pa·s. This comparison in the time domain is carried out in order to show again the robustness of our new ODE method at relatively high viscosities and to underline again the excellent fitting of convolution-integral type unsteady friction models for viscous compressible fluids in flexible pipes. Figs. 34 and 35 show the good agreement between the reference solution and the 1D models implemented with the Kagawa ODE and with the UZ ODE models, respectively.

3.4 Efficiency analysis and computational times

The reference solution for the impedance matrix allows to compute the error and to compare it against the CPU times for the different schemes here considered. The error calculated is intended as the mean of the relative errors between the numerical solution and the analytical one related to the absolute value of the complex parameter z_{11}:

$$\epsilon_{|z_{11}|} = \frac{1}{N_f} \sum_{i=1}^{N_f} \left| \frac{|z_{11}^{num}(f_i)| - |z_{11}^{ex}(f_i)|}{|z_{11}^{ex}(f_i)|} \right| \quad . \tag{52}$$

This analysis has been carried out for a test fluid characterized by $c_0 = 1400$ m/s, $\rho_0 = 998.2$ kg/m^3, and $\mu = 10^{-2}$ Pa/s in a rigid pipe of length $L = 1$ m. Here, the friction model used in the 1D models is the ODE method with the coefficients of Kagawa. First, we consider the error of all first order schemes with three different meshes with $N_x = 100, 250, 500$; for the explicit schemes the time step size Δt is given by the CFL condition with CFL $= 0.9$, while for semi-implicit schemes

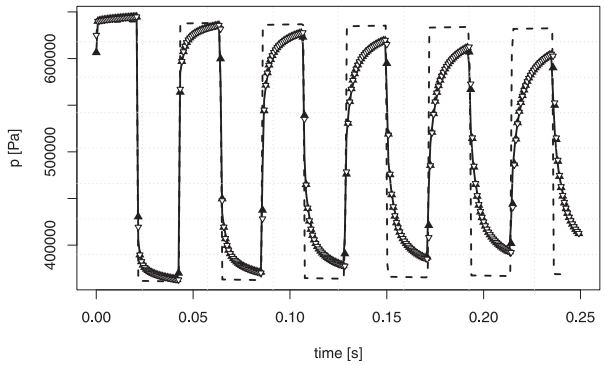

Fig. 30 Water hammer, rigid pipe - Reference solution (—), 1D methods without unsteady friction (- - -), numerical data given by SI1D with Kagawa model (▲) and by PC1D with Kagawa model (▽).

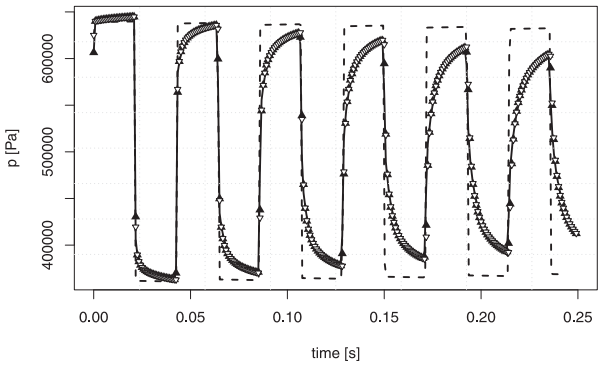

Fig. 31 Water hammer, rigid pipe - Reference solution (—), 1D methods without unsteady friction (- - -), numerical data given by SI1D with Kagawa ODE model (▲) and by PC1D with Kagawa ODE model (▽).

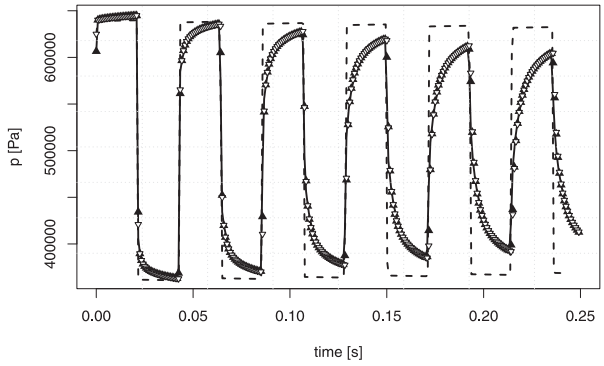

Fig. 32 Water hammer, rigid pipe - Reference solution (—), 1D methods without unsteady friction (- - -), numerical data given by SI1D with UZ model (▲) and by PC1D with UZ model (▽).

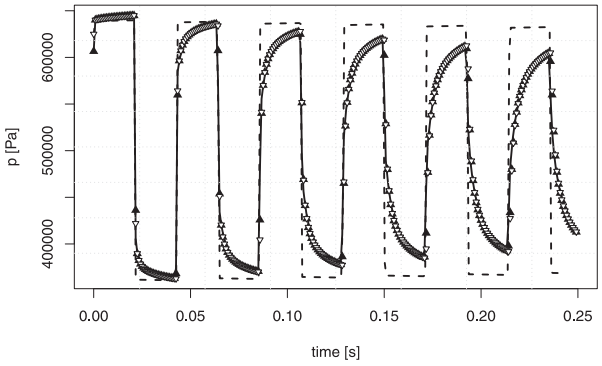

Fig. 33 Water hammer, rigid pipe - Reference solution (—), 1D methods without unsteady friction (- - -), numerical data given by SI1D with UZ ODE model (▲) and by PC1D with UZ ODE model (▽).

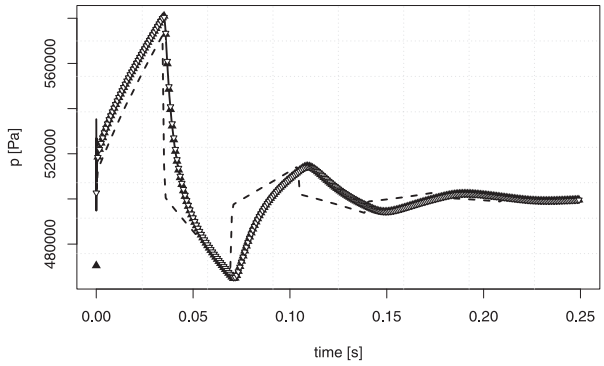

Fig. 34 Water hammer, elastic pipe - Reference solution (—), 1D methods without unsteady friction (- - -), numerical data given by SI1D with Kagawa ODE model (▲) and by PC1D with Kagawa ODE model (▽).

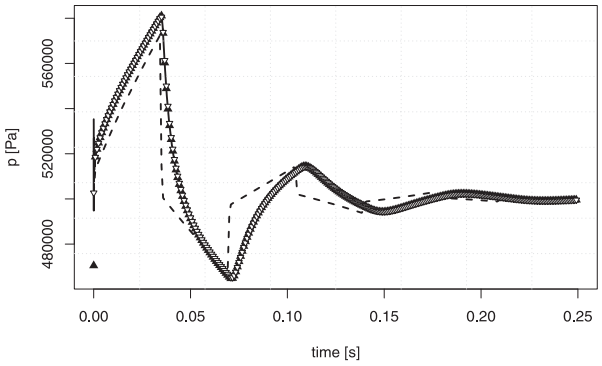

Fig. 35 Water hammer, elastic pipe - Reference solution (—), 1D methods without unsteady friction (- - -), numerical data given by SI1D with UZ ODE model (▲) and by PC1D with UZ ODE model (▽).

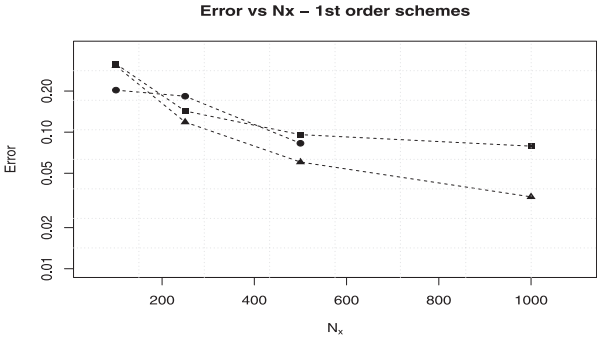

Fig. 36 N_x and errors for the first order schemes - • Explicit schemes, ▲ SI1D, ■ SI2D.

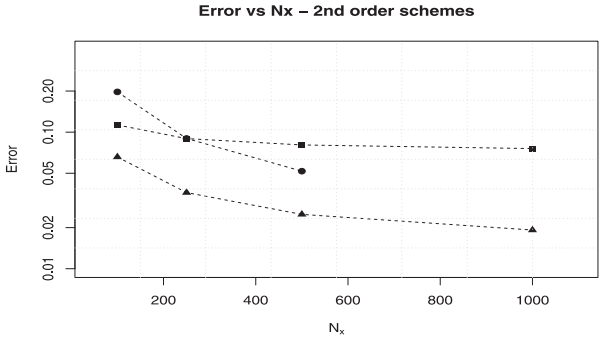

Fig. 37 N_x and errors for the second order schemes - • Explicit schemes, ▲ SI1D, ■ SI2D.

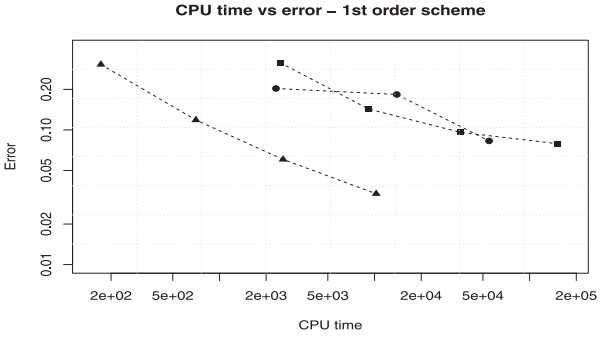

Fig. 38 CPU times and errors for the first order schemes - • Explicit schemes, ▲ SI1D, ■ SI2D.

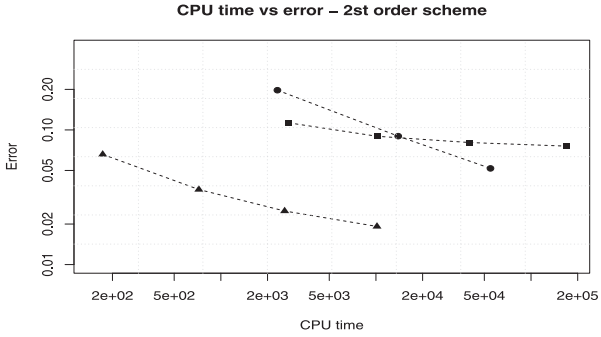

Fig. 39 CPU times and errors for the second order schemes - • Explicit schemes, ▲ SI1D, ■ SI2D.

it is chosen as $\Delta t = T/N_x$, so that a wave period is resolved with N_x time steps (points per wave length). The results of this analysis are given in Table 1. In Fig. 36 it is possible to see that when the number of longitudinal cells increases, the errors decrease. We then have repeated all the simulations using the second order schemes and from Table 1 and from the plot in Fig. 37 it can be observed that the error is much lower than in the first order case, especially for the semi-implicit schemes. Furthermore, in some cases for SI2D the error is also lower than the one of the second order explicit schemes. Moreover, for the semi-implicit schemes we decided to introduce also a grid where N_x is equal to 1000 because experiments have shown that the qualitative solution improved in particular where the parameters $|z_{11}|$ and $|z_{12}|$ have peaks. At the end of this analysis, we decided to simulate the frequency domain with a resolution of 2 mm for the explicit schemes while for the semi-implicit schemes we have chosen $\Delta x = 1$ mm and with time resolution of $T/100$.

Furthermore, the CPU times of the simulations have been plotted against the errors both for the 1st order and for the 2nd order schemes (see Fig. 38 and Fig. 39). In general, for a given error the semi-implicit 1D method gives results in much less time with respect to the explicit 1D scheme and w.r.t. SI2D. For the second order case, SI2D is computationally more efficient than the explicit schemes for a given spatial grid. The computational times of the simulations done for the

Table 1 Frequency domain - error $\epsilon_{|z_{11}|}$ for the first order schemes and for the second order schemes corresponding to different N_x.

		Explicit Scheme		Semi-implicit 1D		Semi-implicit 2D	
N_x	Δx [mm]	$\epsilon_{\lvert z_{11}\rvert}$ 1st order	$\epsilon_{\lvert z_{11}\rvert}$ 2nd order	$\epsilon_{\lvert z_{11}\rvert}$ 1st order	$\epsilon_{\lvert z_{11}\rvert}$ 2nd order	$\epsilon_{\lvert z_{11}\rvert}$ 1st order	$\epsilon_{\lvert z_{11}\rvert}$ 2nd order
100	10	0.2031	0.1972	0.3061	0.0658	0.3157	0.1129
250	4	0.1833	0.0899	0.1185	0.0361	0.1428	0.0897
500	2	0.0529	0.0518	0.0604	0.0250	0.0959	0.0806
1000	1	-	-	0.0336	0.0192	0.0790	0.0758

Table 2 Frequency domain - CPU times for the first order schemes and for the second order schemes corresponding to different N_x.

CPU time [s]		Explicit Scheme		Semi-implicit 1D		Semi-implicit 2D	
N_x	Δx [mm]	1st order	2nd order	1st order	2nd order	1st order	2nd order
100	10	1989	2315	172	173	2462	2741
250	4	11742	13923	705	721	9177	10171
500	2	39810	54776	2574	2578	35962	40208
1000	1	-	-	10246	10158	151680	169475

Table 3 CPU times in seconds for the two-dimensional method compared with different one dimensional methods.

SI2D	Impedance matrix (Rigid pipe) 50550			Impedance matrix (Elastic pipe) 66059			Water hammer (Rigid) 227		
1D	SI1D	PC Osher	PC HLL	SI1D	PC Osher	PC HLL	SI1D	PC Osher	PC HLL
Trikha	784	37575	39623	1391	419309	549111	16	121	193
Kagawa	1204	40408	41594	1968	405697	552679	28	135	207
Kagawa ODE	832	38030	39630	1483	405517	552166	22	127	200
UZ	3143	45037	46536	3387	426222	578988	56	164	239
UZ ODE	2503	39988	40145	2115	422963	583574	38	141	219
Brunone	863	37233	40272	1352	415219	573813	15	120	193

impedance matrix and for the water hammer have been measured and they are exposed in Table 3 for SI2D and for the one dimensional schemes.

It is possible to observe that for the impedance matrix for the rigid tube the CPU time of the scheme SI2D is very similar to the one of the explicit 1D methods both with the Osher RS and with the HLL RS. However, for the elastic case the 1D explicit method becomes extremely slow (due to the necessary iterative computation of the primitive variables from the vector of conserved quantities), and one can observe that the two dimensional *semi-implicit* method is almost one order of magnitude *faster* than the *explicit* 1D methods, which is quite a remarkable result. Moreover, the experiments done using the Osher RS have produced the results in less time with respect to the HLL RS. This last fact occurs because the iterative procedure for the calculation of the pressure ($g(p) = Q_1 - \rho(p)A(p)$) is required more times in the computation of the HLL flux than in the evaluation of the Osher flux. We think this is a very particular case for this non-linear system of PDEs studied in this paper. For systems composed by more than 2 PDEs the Osher RS is in general more expensive. Anyway, for all the test cases the method SI1D is clearly the fastest of the schemes that have been considered here, since it represents a special case of SI2D when $N_r = 1$; it gives very accurate results in a very small computational time. Last but not least, in all simulations we observe that our new ODE integrator method (45) for the Zielke convolution integral is faster than the original formula of Kagawa. This is valid using both, the Kagawa coefficients as well as the Urbanowicz and Zarzycky coefficients. We attribute this result to the fact that the new ODE method does not involve time-consuming evaluations of exponential functions.

4 Conclusions

In this paper we have implemented several finite volume schemes for the system of partial differential equations that govern pressurized viscous compressible flows in rigid and flexible pipes. The classical explicit Godunov-type schemes have to be supplemented by using a path conservative approach in order to consider the varying cross section due to the elastic wall deformation. Another family of methods under consideration is the class of staggered semi-implicit finite volume schemes.

For this class of methods, the two-dimensional case gives accurate results without the need of any closure for the viscous term. Furthermore, in most cases the 2D semi-implicit method is almost as fast as the explicit one-dimensional scheme, but in some cases it can even be faster.

Moreover, in order to match the exact solution and the experimental measurements, all one dimensional models need a closure relation for the wall friction, in particular for the unsteady contribution to the wall shear stress that is crucial for the simulations that have been considered here. Several unsteady friction models have been incorporated into the 1D schemes. The thorough comparisons have shown that the models of Brunone and of Trikha do not give a good fitting, especially when the viscosity assumes large values. The most accurate models seem to be those that approximate the convolution integral of Zielke, such as the model of Kagawa and the one Urbanowicz and Zarzycki. Furthermore, we have proposed a new formula for the evaluation of the integral of Zielke, which is as accurate as the formula of Kagawa, but it is faster since it does not involve the time consuming evaluation of exponential functions.

Further work will regard investigations of the friction effects considering the full compressibility of the fluid including the energy equation, more complex tube laws for the wall deformation and an extension to higher order of accuracy following recent developments on semi-implicit staggered DG schemes presented in [11, 30, 31].

Acknowledgements The research presented in this paper was funded by the company Robert Bosch GmbH, Germany. The authors want to thank Dr.-Ing. Ronny Leonhardt, who supplied the experimental and analytical reference solutions for the impedance matrix for the rigid and elastic tube. Moreover, the authors are grateful to Dipl.-Inf. Julia Leibinger, who suggested many literature references.

References

[1] L. Brugnano and V. Casulli, Iterative solution of piecewise linear systems, SIAM J. Sci. Comput. **30**, 463–472 (2008).
[2] L. Brugnano and V. Casulli, Iterative solution of piecewise linear systems and applications to flows in porous media, SIAM J. Sci. Comput. **31**, 1858–1873 (2009).
[3] B. Brunone, U. M. Golia, and M. Greco, Modelling of fast transients by numerical methods, Proc. Int. Conference on Hydr. Transients with Water Column Separation, 273–280 (1991).
[4] B. Brunone, U. M. Golia, and M. Greco, Some remarks on the momentum equation for fast transients. In: Proc. Int. Conference on Hydr. Transients with Water Column Separation, 201–209 (1991).
[5] M. Castro, J. Gallardo, and C. Parés, High-order finite volume schemes based on reconstruction of states for solving hyperbolic systems with nonconservative products. Applications to shallow-water systems, Math. Comput. **75**, 1103–1134 (2006).
[6] M. Castro, J. Gallardo, and A. Marquina, Approximate Osher–Solomon schemes for hyperbolic systems, Appl. Math. Comput. **272**, 347–368 (2016).
[7] M. Castro, A. Pardo, C. Parés, and E. Toro, On some fast well-balanced first order solvers for nonconservative systems, Math. Comput. **79**, 1427–1472 (2010).
[8] V. Casulli, M. Dumbser, and E. F. Toro, Semi-implicit numerical modeling of axially symmetric flows in compliant arterial systems, Int. J. Numer. Methods Biomed. Eng. **28**, 257–272 (2012).
[9] V. Casulli and P. Zanolli, A nested Newton-type algorithm for finite volume methods solving Richard's equation in mixed flow, SIAM J. **32**, 2255–2273 (2009).
[10] V. Casulli and P. Zanolli, Iterative solution of mildly nonlinear systems, J. Comput. Appl. Math. **236**, 3937–3947 (2012).
[11] M. Dumbser and V. Casulli, A staggered semi-implicit spectral discontinuous Galerkin scheme for the shallow water equations, Appl. Math. Comput. **219**, 8057–8077 (2013).
[12] M. Dumbser and V. Casulli, A conservative, weakly nonlinear semi-implicit finite volume scheme for the compressible Navier-Stokes equations with general equation of state, Appl. Math. Comput. **272**, 479–497 (2016).
[13] M. Dumbser and D. S. Balsara, A new efficient formulation of the HLLEM Riemann solver for general conservative and non-conservative hyperbolic systems, J. Comput. Phys. **304**, 275–319 (2016).
[14] M. Dumbser, U. Iben, and M. Ioriatti, An efficient semi-implicit finite volume method for axially symmetric compressible flows in compliant tube, Appl. Numer. Math. **89**, 24–44 (2015).
[15] M. Dumbser, U. Iben, and C. D. Munz, Efficient implementation of high order unstructured WENO schemes for cavitating flows, Comp. Fluids **86**, 141–168 (2013).
[16] M. Dumbser and E. F. Toro, On universal Osher-type schemes for general nonlinear hyperbolic conservation laws, Commun. Comput. Phys. **10**, 635–671 (2011).
[17] F. Fambri, M. Dumbser, and V. Casulli, An efficient semi-implicit method for three-dimensional non-hydrostatic flows in compliant arterial vessels, Int. J. Numer. Method. Biomed. Eng. **30**, 1170–1198 (2014).
[18] M. Goeke, Modellierung der Materialdämpfung bei der Wellenausbreitung in flexiblen Leitungen. Institut für Baustatik und Baudynamik der Universität Stuttgart, (2013).
[19] E. Han, M. Hantke, and G. Warnecke, Exact Riemann solutions to compressible Euler equations in ducts with discontinuous cross-section, Journal of Hyperbolic Differential Equations **9**, 403–449 (2012).
[20] E. L. Holmboe and W. T. Rouleau, The effects of viscous shear on transients in liquid lines, J. Basic Eng. **89**, 174–180 (1967).
[21] T. Kagawa, I. Lee, A. Kitagawa, and T. Takenaka, High speed and accurate computing method of frequency-dependent friction in laminar pipe flow for characteristics method, Trans. Jpn. Soc. Mech. Eng. Ser. **49**, 2638–2644 (1983).

[22] J. Leibinger, M. Dumbser, U. Iben, and I. Wayand, A path-conservative Osher-type scheme for simulating axially symmetric compressible flows in flexible visco-elastic tubes, Appl. Numer. Math. **105**, 47–63 (2016).
[23] R. Leonhardt, Dynamische Untersuchungen von Hydraulikkomponenten, Fakultät für Maschinenbau der Universiät Karlsruhe, (2008).
[24] P. Moczo and J. Kristek, On the rheological model used for time-domain methods of seismic wave propagation, Geophys. Res. Lett. **32**, L01306 (2005).
[25] S. Osher, Riemann solver, the entropy condition and difference approximations, SIAM J. Numerical. Anal. **21**, 217–235 (1984).
[26] S. Osher and F. Solomon, Upwind difference schemes for hyperbolic systems: a theoretical framework, Math. Comput. **38**, 339–374 (1982).
[27] C. Parés, Numerical methods for nonconservative hyperbolic systems: a theoretical framework, SIAM J. Numer. Anal. **44**, 300–321 (2006).
[28] G. Pezzinga, Evaluation of unsteady flow resistances by quasi-2D or 1D models, J. Hydraul. Eng. **126**, 778–785 (2000).
[29] D. Rochette, S. Clain, and W. Bussière, Unsteady compressible flow in ducts with varying cross-section: Comparison between the non-conservative Euler system and the axisymmetric flow model, Computers and Fluids **53**, 53–78 (2012).
[30] M. Tavelli and M. Dumbser, A staggered semi-implicit discontinuous Galerkin method for the two dimensional incompressible Navier-Stokes equations, Appl. Math. Comput. **248**, 70–92 (2014).
[31] M. Tavelli and M. Dumbser, A staggered space-time discontinuous Galerkin method for the incompressible Navier-Stokes equations on two-dimensional triangular meshes, Computers and Fluids **119**, 235–249 (2015).
[32] M. Tavelli, M. Dumbser, and V. Casulli, High resolution methods for scalar transport problems in compliant systems of arteries, Appl. Numer. Math. **74**, 62–82 (2013).
[33] E. F. Toro, Riemann Solvers and Numerical Methods for fluid Dynamics, third ed. (Springer, 2009).
[34] A. K. Trikha, An efficient method for simulating frequency-dependent friction in transient liquid flow, J. Fluid Eng. **97**(1), 97–105 (1975).
[35] K. Urbanowicz and Z. Zarzycki, New efficient approximation of weighting functions for simulations of unsteady friction losses in liquid pipe flow, J. Theor. Appl. Mech. **20**, 487–508 (2012).
[36] B. van Leer, Towards the ultimate conservative difference scheme V. A second-order sequel to Godunov's methods, J. Comput. Phys. **32**, 101–136 (1979).
[37] A. E. Vardy and J. M. Brown, On turbulent, unsteady, smooth-pipe friction, Proc. of the 8th International Conf. on Pressure Surges - BHR Group, The Hague, 289–311 (1996).
[38] A. E. Vardy and J. M. Brown, Efficient approximation of unsteady friction weighting functions, J. Hydraul. Eng. **130**, 1219–1228 (2004).
[39] J. P. Vtkovsky, M. L. Stephens, A. Bergant, A. R. Simpson, and M. F. Lambert, Efficient and accurate calculation of Zielke and Vardy-Brown unsteady friction in pipe transient, 9th Conference on Pressure Surges, Chester (UK), (2004).
[40] J. Womersley, Method for the calculation of velocity, rate of flow and viscous drag in arteries when the pressure gradient is known, J. Physiol. **127**, 553–563 (1955).
[41] W. Zielke, Frequency-dependent friction in transient pipe flow, J. Basic Eng. **90**, 109–115 (1968).

